energies

MDPI

Article

CO_2 Storage Site Assessment in the Mugrosa Formation, Middle Magdalena Valley Basin: An Integrated Geocellular, Geomechanical, and Fault Seal Modeling Workflow

Edwar Herrera Otero [1,*] and Maria Cecilia Ruiz Cardona [2]

[1] School of Petroleum Engineering, Faculty of Physicochemical Engineering, Universidad Industrial de Santander, Bucaramanga 680002, Colombia
[2] Agencia Nacional de Hidrocarburos, Bogotá 110221, Colombia; maria.ruiz@anh.gov.co
* Correspondence: edherote@uis.edu.co

Abstract

Geological CO_2 storage represents one of the main strategies for mitigating greenhouse gas emissions within the framework of global energy transition. This study presents an integrated workflow for assessing the geological CO_2 storage potential of the Mugrosa Formation in the Middle Magdalena Valley Basin (Colombia). The methodology integrates multicriteria analysis, seismic interpretation, sedimentological and petrophysical characterization, three-dimensional geocellular modeling, geomechanical analysis, and fault seal evaluation using Shale Gouge Ratio (SGR) approach to assess reservoir-seal integrity and storage feasibility. Based on regional evaluation, two targets were selected: North and Central Structures. Seismic interpretation identified faulted anticline traps associated with reverse faults within a compressional regime, revealing different degrees of reservoir compartmentalization. Petrophysical characterization showed a predominance of clay-rich facies, with shale volume > 90% in some intervals, limiting reservoir quality and restricting storage potential to discrete sandy bodies. Reservoir intervals exhibit effective porosity from 13–15% and permeability between 500–800 mD. Geomechanical analysis allowed the evaluation of system stability under injection conditions, main faults are close to critical reactivation conditions, although they remain stable under moderate injection pressures. High SGR values (>0.75) suggest favorable fault-sealing capacity. Storage feasibility is controlled by the balance between reservoir quality, structural integrity, and geomechanical behavior. The integrated workflow provides a robust framework for subsurface integrity assessment and early-stage screening of geological CO_2 storage prospects in structurally complex sedimentary basins.

Keywords: CO_2 geological storage; geocellular modeling; reservoir characterization; fault seal analysis; Shale Gouge Ratio (SGR); geomechanical modeling

Check for updates

Academic Editor: Andrea De Pascale

Received: 9 July 2026
Revised: 31 July 2026
Accepted: 17 August 2026
Published: 2 September 2026

Copyright: © 2026 by the authors. Licensee MDPI, Basel, Switzerland. This article is an open access article distributed under the terms and conditions of the Creative Commons Attribution (CC BY) license.

1. Introduction

Geological CO_2 storage has become one of the main strategies for mitigating greenhouse gas emissions within the context of the global energy transition and the development of Carbon Capture and Storage (CCS) technologies [1,2]. Its long-term feasibility largely depends on the subsurface capacity to safely and permanently contain injected CO_2, which requires a comprehensive characterization of the reservoir-seal system and a rigorous assessment of subsurface integrity under injection conditions [3].

Traditionally, the evaluation of geological storage sites has been conducted through independent analyses focused separately on structural, petrophysical, geomechanical, or seal-capacity aspects [4]. Although these approaches are widely applied, they present important limitations because they do not fully capture the coupled interaction between reservoir heterogeneity, mechanical behavior, and fault response to pore-pressure changes induced by CO_2 injection [5,6].

In structurally complex sedimentary basins, structural characterization defines trap geometries, compartmentalization, and fault architecture, whereas geocellular modeling enables the spatial representation of facies distribution and petrophysical heterogeneity within the storage interval [7]. In parallel, geomechanical analysis evaluates the stability of the reservoir-seal system under stress perturbations associated with injection processes, while fault seal assessment methods, such as the Shale Gouge Ratio (SGR), provide quantitative estimations of the sealing behavior of faults and their capacity to act as hydraulic barriers [8]. However, the isolated application of these methodologies limits a holistic understanding of containment risk, particularly in heterogeneous reservoirs affected by complex structural deformation [9].

Consequently, there is still a need for integrated methodologies capable of simultaneously evaluating: (i) the spatial heterogeneity of the reservoir, (ii) the mechanical stability of the system during injection, (iii) fault behavior and reactivation potential, and (iv) the sealing capacity of structural discontinuities.

The integration of these components within a unified modeling framework represents a critical step toward improving reliability in the screening, selection, and risk assessment of geological CO_2 storage sites. Recent studies have highlighted that thermo-mechanical coupling, stress redistribution, and fracture evolution may significantly influence the long-term performance and integrity of subsurface storage systems [10,11].

In this context, the Middle Magdalena Valley Basin in Colombia constitutes a promising region for future Carbon Capture, Utilization and Storage (CCUS) applications due to its favorable geological conditions, hydrocarbon infrastructure, and proximity to major industrial CO_2 emission sources [12]. Among the potential storage units, the Mugrosa Formation represents an attractive target because of its stratigraphic configuration, structural trapping conditions, and the presence of interbedded reservoir and sealing facies.

This study proposes and applies an integrated workflow that combines three-dimensional geocellular modeling, geomechanical analysis, and fault seal assessment to quantify subsurface integrity in a CO_2 geological storage scenario within the Mugrosa Formation. The proposed approach explicitly links reservoir heterogeneity, structural configuration, mechanical stability, and fault-sealing behavior within a single geocellular framework.

The main contribution of this work lies in the development of a unified methodological framework that integrates geological, petrophysical, structural, and geomechanical domains into a consistent subsurface model for CO_2 storage site assessment. This integrated approach not only improves the characterization of containment-related risks but also provides a more robust basis for prospect ranking and decision-making during the early stages of screening CCUS project evaluation.

2. Geological Setting of the Middle Magdalena Valley Basin

2.1. Basin Architecture and Tectonic Evolution

The Middle Magdalena Valley Basin (MMVB) is an intermontane depression located between the Central and Eastern Cordilleras of Colombia and represents one of the most structurally complex sedimentary systems within the Northern Andes due to its prolonged tectonostratigraphic evolution. Its present-day configuration results from the superposition

of Mesozoic extensional tectonics and Cenozoic compressional deformation, generating an inherited structural framework that was subsequently inverted and now controls the geometry of subsurface units [13,14].

During the Late Triassic-Jurassic, the basin evolved under an extensional tectonic regime associated with intracontinental rifting processes linked to the regional fragmentation of the northwestern South American margin. This stage promoted the formation of hemigrabens and the accumulation of continental syn-rift successions, establishing a structural basement that later conditioned Andean deformation. Subsequently, during the Cretaceous, the basin underwent thermal subsidence and developed as a passive to back-arc margin environment, characterized by widespread marine sedimentation and the deposition of regionally extensive carbonate and siliciclastic successions [15].

From the Paleogene onward, and particularly during the Miocene, Andean convergence induced a transition toward a compressional tectonic regime, promoting the tectonic inversion of pre-existing extensional structures. This process generated a structural style dominated by reverse faults, associated folds, and thrust systems, especially along the eastern margin of the basin. The selective reactivation of paleo-normal faults produced complex structural configurations and significant subsurface compartmentalization [16].

As a result, the MMVB is currently recognized as an inverted intermontane basin with sedimentary thicknesses exceeding several kilometers and marked structural and stratigraphic heterogeneity. The predominant NNE-SSW orientation of faults and folds reflects the combined influence of Andean tectonics and Mesozoic structural inheritance [17]. These characteristics are particularly relevant for geological CO_2 storage applications because they directly influence reservoir continuity, fault connectivity, mechanical stability, and the sealing integrity of the reservoir-seal system.

In this context, understanding the tectonic evolution of the MMVB is essential for evaluating the viability of reservoir-seal systems, identifying structurally favorable storage zones, and anticipating potential migration pathways induced by CO_2 injection. Therefore, the inherited structural architecture of the basin constitutes a key factor in the integrated risk assessment of deep geological CO_2 storage projects.

2.2. Stratigraphic Framework of the Target Reservoir-Seal System Formations

The sedimentary succession of the Middle Magdalena Valley Basin comprises a series of Paleogene and Neogene units with lithological and petrophysical characteristics favorable for deep geological storage applications. Within this framework, the Mugrosa, Colorado, and Esmeraldas formations constitute a stratigraphic system of particular interest due to their vertical arrangement, internal heterogeneity, and functional relationships within the reservoir-seal architecture.

These units represent continental to transitional depositional environments developed during the Cenozoic evolution of the basin and are associated with fluvial, deltaic, and alluvial plain systems [17]. Their lateral and vertical variability reflects changes in subsidence patterns, sediment supply, and tectonic controls, resulting in a complex stratigraphic architecture characterized by interbedded sandstone and mudstone intervals that strongly influence subsurface hydraulic behavior. Collectively, these formations provide favorable geological configurations for CO_2 storage, where porous sandy intervals act as potential storage reservoirs, while overlying fine-grained successions perform sealing functions.

From a subsurface engineering perspective, the assessment of these units requires consideration not only of their individual petrophysical properties but also of their stratigraphic connectivity, lateral continuity, and capacity to maintain long-term confinement conditions at the regional scale. In this study, these formations were selected as the primary

target interval because of their representativeness within the regional petroleum system and their potential applicability for geological CO_2 storage in mature sedimentary basins.

2.2.1. Mugrosa Formation

The Mugrosa Formation is an Early to Middle Miocene siliciclastic unit widely distributed throughout the Middle Magdalena Valley Basin. It is predominantly composed of fine- to medium-grained sandstones interbedded with siltstones, claystones, and carbonaceous levels, reflecting deposition within meandering fluvial systems influenced by extensive floodplain environments [18].

From a petrophysical perspective, the Mugrosa Formation represents one of the principal reservoir intervals in the basin due to its moderate-to-high effective porosity and variable permeability, which are strongly controlled by facies distribution and diagenetic cementation processes. The internal heterogeneity of the formation promotes local reservoir compartmentalization while simultaneously favoring the development of laterally connected sandstone bodies capable of storing significant fluid volumes [18].

For geological CO_2 storage applications, the Mugrosa Formation constitutes a strategic target because of its potential injectivity and its stratigraphic position within a system overlain by lower-permeability units. However, its storage performance is critically dependent on the lateral continuity of sandy bodies, the degree of structural compartmentalization, and the interaction with active or reactivated fault systems that may influence pressure distribution and fluid migration pathways.

2.2.2. Colorado Formation

The Miocene Colorado Formation is characterized by a succession of sandstones, shales, and siltstones deposited within fluvio-deltaic to transitional depositional environments. Its sedimentary architecture reflects significant lateral variability associated with channel migration processes and fluctuations in sediment supply regimes [18].

From a functional perspective, the Colorado Formation may act both as a secondary reservoir unit and as a hydraulic transition interval within the regional stratigraphic framework. The sandstone bodies exhibit locally favorable storage properties, although they generally present greater heterogeneity than those observed in the Mugrosa Formation. The occurrence of interbedded clay-rich intervals increases the complexity of vertical fluid flow and may contribute to localized sealing and pressure compartmentalization within the system [19].

Its relevance in the present study lies in its role as an intermediate stratigraphic unit, whose detailed characterization is necessary to evaluate vertical connectivity, potential migration pathways, and pressure distribution under CO_2 injection scenarios.

2.2.3. Esmeraldas Formation

The Esmeraldas Formation is a predominantly fine-grained unit deposited in low-energy continental environments and is mainly composed of shales, claystones, and siltstones with subordinate intercalations of fine-grained sandstones [19]. Its broad regional distribution and limited occurrence of permeable facies make it a key component of the regional confinement system [17].

From a geological storage perspective, the Esmeraldas Formation performs a fundamental role as a regional seal, restricting the vertical migration of fluids and providing both capillary and mechanical barriers above the underlying intervals. Its thickness and lateral continuity constitute critical parameters in subsurface integrity assessment and long-term containment evaluation.

Additionally, its geomechanical properties, including relatively higher ductility and lower permeability, favor stress dissipation and reduce the risk of injection-induced fracturing, increasing its relevance under prolonged CO_2 injection scenarios.

2.3. Structural Framework and Implications for CO_2 Storage Integrity

The structural framework of the Middle Magdalena Valley Basin exerts a primary control on the geometry, continuity, and hydraulic behavior of subsurface systems evaluated for geological CO_2 storage. The present-day configuration of the basin reflects a predominantly compressional tectonic regime resulting from the Cenozoic inversion of pre-existing Mesozoic extensional structures [20]. This tectonic evolution generated a complex network of reverse faults, associated folds, and thrust systems that segment the subsurface and control the architecture of structural traps and sealing barriers at multiple scales [21].

Within the study area, seismic interpretation integrated with well data revealed a structural pattern dominated by high-angle faults with preferential NNE-SSW and NE-SW orientations, consistent with regional Andean deformation trends. These structures define partially compartmentalized tectonic blocks and generate anticline and homoclinal configurations favorable for fluid accumulation and containment.

From a geological storage perspective, faults represent a dual-control element within the subsurface system. On one hand, faults may act as hydraulic barriers when characterized by clay-rich gouge zones, favorable seal-reservoir juxtapositions, and low reactivation potential. On the other hand, they may constitute preferential migration pathways if vertically connected or if they experience mechanical integrity loss under injection-induced overpressure conditions.

Therefore, structural integrity assessment requires the simultaneous evaluation of fault geometry, kinematic evolution, petrophysical properties, and geomechanical response under injection scenarios. In this context, methodologies such as Shale Gouge Ratio (SGR), fault seal analysis, and effective stress stability criteria are essential for estimating sealing capacity and leakage risk associated with major structural discontinuities.

Additionally, the interaction between folded structures and stratigraphic heterogeneity generates internal reservoir compartmentalization, affecting pressure distribution and storage efficiency. This compartmentalization may be advantageous by limiting the regional propagation of the CO_2 plume; however, it also increases operational complexity by requiring differentiated injection and monitoring strategies.

In mature compressional systems such as the Middle Magdalena Valley Basin, storage integrity does not depend exclusively on reservoir quality or regional seal thickness, but rather on the coupled response between structural architecture, mechanical properties, and hydraulic connectivity. Consequently, the structural framework must be considered a central component in risk assessment and prospect selection for deep geological CO_2 storage applications.

From an operational perspective, the identification of structurally favorable sectors involves prioritizing areas with lower fault density, reduced fault reactivation probability, adequate separation between critical faults and injection trajectories, and sufficient lateral continuity of the overlying sealing units. This approach contributes to reducing uncertainty and strengthening decision-making robustness during the early planning stages of CCS projects.

3. Methodology

This study proposes a methodological framework for assessing geological CO_2 storage potential based on reservoir modeling approaches widely applied in the hydrocarbon industry and adapted to a deterministic storage-capacity estimation scheme. The method-

ology is structured into a sequence of integrated stages leading to the comprehensive characterization of the reservoir-seal system, the identification of prospective storage units, and the development of a three-dimensional geocellular model.

The proposed geocellular model consistently integrates structural, stratigraphic, petrophysical, geomechanical, and fault-sealing domains within a unified subsurface framework. The sedimentological component is based on facies analysis and characterization, enabling the definition of spatial property distributions consistent with the depositional environment and stratigraphic architecture of the system. This multiscale integration approach allows the representation of reservoir heterogeneity, reduces uncertainty associated with spatial property distribution, and establishes a robust basis for evaluating storage capacity and subsurface integrity under CO_2 injection scenarios.

3.1. Study Area Definition and Reservoir Ranking

The study area was defined through a sequential screening approach following the methodology proposed by Bachu (2000) [22]. In the first stage, preliminary target areas were identified based on their proximity to one of the main industrial CO_2 emission sources in Colombia, the Barrancabermeja Refinery. A 100 km (km) radius buffer zone was established around the emission source, within which only areas classified as available by the National Hydrocarbons Agency (ANH) were selected, ensuring the operational and regulatory feasibility of the assessment.

Subsequently, the multicriteria evaluation methodology proposed by Bachu (2003) [23] and Bachu and Adams (2003) [24] were applied. This approach is based on a normalized scoring system that integrates 15 evaluation parameters to generate an overall suitability ranking. The methodology allows the prioritization of prospective areas according to their suitability for geological CO_2 storage, considering geological, structural, thermodynamic, and operational variables.

3.2. Compilation and Review of Available Data

The primary dataset comprises well-log data from 48 exploration and development wells, including gamma ray (*GR*), Spontaneous Potential (SP), resistivity, bulk density (RHOB), and Neutron Porosity (NPHI) logs. In addition, 34 two-dimensional seismic lines acquired from seven independent seismic surveys were integrated into the study, representing approximately 391 km of total seismic coverage. This dataset provided an adequate spatial framework for the structural and stratigraphic interpretation of the study area.

3.3. Reservoir Characterization

Reservoir characterization was conducted through the integrated analysis of sedimentological and petrophysical information with the objective of defining the spatial distribution of facies and porous-medium properties within the geocellular model [25]. This process constitutes the basis for representing reservoir heterogeneity and for the subsequent estimation of geological CO_2 storage capacity.

3.3.1. Sedimentological Characterization and Facies Definition

Sedimentological characterization was performed through the integration of thin-section petrographic analysis and well-log interpretation. This approach allowed the identification of facies associations and the definition of their vertical and lateral distribution within the target stratigraphic units.

Core analysis included the description of lithology, texture, sedimentary structures, and stratigraphic contacts, enabling the identification of dominant depositional environments associated with fluvial and alluvial plain systems. Complementarily, petrographic

analysis was used to evaluate mineralogical composition, matrix type, degree of cementation, and pore-system characteristics, providing key information for diagenetic interpretation and its impact on reservoir quality.

The interpretation of well logs, particularly *GR* and SP, was used to extend facies classification into intervals lacking core control. Based on the response patterns of these logs, electro facies were defined through the identification of characteristic signatures associated with specific lithologies.

Based on this integrated workflow, a representative facies scheme of the depositional system was established and subsequently discretized within the geocellular model [26]. This classification enabled the representation of sedimentary heterogeneity and the establishment of consistent relationships between facies distribution and petrophysical properties.

3.3.2. Petrophysical Characterization

Petrophysical characterization was conducted to estimate the fundamental reservoir properties, including shale volume, effective porosity, and fluid saturation, through the analysis of well-log data.

Whenever available, petrophysical parameters were calibrated using laboratory core measurements, including porosity and permeability data. This calibration process allowed the adjustment of log responses and improved the reliability of petrophysical estimations [27].

The derived properties were subsequently integrated into the geocellular model through interpolation and geostatistical simulation techniques while honoring the previously defined facies distribution. This workflow enabled the construction of consistent three-dimensional petrophysical models, which constitute a fundamental input for evaluating reservoir behavior under CO_2 injection conditions.

3.4. Seismic Interpretation and Structural Model

Seismic interpretation was performed using Petrel 2021 software, following a workflow that included seismic-to-well tie calibration, horizon and fault interpretation, and time-to-depth conversion. During this stage, key stratigraphic horizons corresponding to the Eocene unconformity, the Esmeraldas, Mugrosa, and Colorado formations, as well as the Cretaceous basement, were identified and mapped.

The structural model was constructed through the integration of interpreted faults, stratigraphic horizons, and regional structural features within the study area, following the Pillar Gridding workflow implemented in Petrel [25]. This workflow enabled the generation of a structurally consistent three-dimensional framework that served as the basis for subsequent facies, petrophysical, and geomechanical modeling.

3.5. Petrophysical Model Construction

Petrophysical evaluation involved the estimation of shale volume from *GR* logs, calculated using Equation (1). The selection of clean-shale and shale reference values was based on the statistical distribution of the dataset, considering the first quintile as representative of the clean interval and the fifth quintile as representative of the shale interval [28].

$$Vsh\ GR = \frac{GR\ log - GR\ clean}{GR\ sh - GR\ clean} \quad (1)$$

where:

Vsh GR is the shale volume estimated from the gamma ray log;

GR log is the gamma ray value at a given depth within the formation;

GR clean is the baseline gamma ray response associated with clean reservoir intervals characterized by minimal shale content;

GR sh is the reference gamma ray value corresponding to the shale interval.

Total porosity (ϕD) was calculated from the density log (*RHOB*) according to Equation (2) [29].

$$\varnothing D = \frac{RHOBma - RHOBl}{RHOBma - RHOBf} \quad (2)$$

where:

$\varnothing D$ = total porosity calculated from the density log

$RHOBma$ = formation matrix density (2.65 and 2.71 g/cc)

$RHOBf$ = fluid density (1 g/cc)

$RHOBl$ = log value (g/cc)

The effective porosity (*PHIE*) is calculated with the following equation:

$$PHIE = \varnothing D \times (1 - vsh), \quad (3)$$

Permeability was subsequently estimated using empirical correlations calibrated according to the available petrophysical information. To estimate the water saturation the Indonesian equation was employed:

$$\frac{1}{\sqrt{Rt}} = \left(\sqrt{\frac{\varnothing^m}{\alpha \times Rw}} + \frac{Vsh^{1-vhs/2}}{\sqrt{Rcl}} \right) \times Sw^{\frac{n}{2}} \quad (4)$$

where:

Rt = formation resistivity (well log)

Rcl = clay resistivity

Rw = water resistivity

α = tortuosity exponent

m = cementation exponent

n = saturation exponent

$\varnothing$ = porosity

Sw = water saturation

Vsh = shale volume

3.6. Fault Seal Analysis Methodology: Shale Gouge Ratio (SGR)

Fault-sealing capacity was evaluated using the Shale Gouge Ratio (SGR) methodology proposed by Yielding et al. (1997) [8]. The SGR estimates the proportion of clay-rich material entrained within the fault zone as a consequence of fault displacement, and is shown as Equation (5).

$$\text{SGR} = \Sigma\ (Vsh \times \Delta z)/\text{T}, \quad (5)$$

where:

Vsh is the shale volume associated with each stratigraphic interval;

Δz is the thickness of each stratigraphic layer;

T is the total vertical fault throw.

SGR values below 0.18–0.25 are commonly interpreted as indicative of limited membrane sealing capacity, whereas values above 0.25 suggest favorable conditions for fault seal development. Although SGR has been widely validated for hydrocarbon systems [8,30], its application to geological CO_2 storage should be interpreted with caution because the CO_2-brine system exhibits different capillary properties than conventional hydrocarbon-water

systems. Therefore, SGR was used as a qualitative indicator of fault-sealing potential and was complemented by capillary breakthrough pressure calculations through the estimation of the maximum sustainable CO_2 column height (Section 3.8, below).

3.7. Geomechanical Analysis

A one-dimensional (1D) geomechanical model was constructed to define the operationally safe injection pressure window and to evaluate the fault reactivation potential. The orientations and magnitudes of the principal stresses were estimated from wellbore breakout data, drilling-induced fractures, and leak-off test (LOT) measurements. Pore pressure was derived from density logs and regional pressure-gradient information. Fault stability was evaluated using the Mohr-Coulomb failure criterion showed at the Equation (6).

$$\tau = c + \mu\,(\sigma n - Pp), \quad (6)$$

where:

τ is the shear stress;
c is rock cohesion;
μ is the friction coefficient;
σn is the normal stress acting on the fault plane;
Pp is the pore pressure.

Rock elastic properties, including Young's modulus and Poisson's ratio, were estimated using Castagna's empirical relationships derived from sonic and density log responses from the Zarzal-2 well, after prior quality control and data validation procedures.

3.8. Estimation of Maximum CO_2 Column

The maximum height of the CO_2 column confined by the sealing formation (Hmáx) was calculated using the capillary entry pressure of the seal rock according to Equation (7):

$$Hmáx = (2\gamma \cos\theta)/(r \times g \times (\rho\ \text{brine} - \rho\ CO_2)), \quad (7)$$

where:

γ is the interfacial tension between CO_2 and brine;
θ is the contact angle;
r is the pore-throat radius;
g is the gravitational acceleration;
ρ brine and ρ CO_2 are the densities of brine and CO_2, respectively.

CO_2 density under reservoir conditions was estimated from the pressure-temperature density charts proposed by Bachu (2003) [23], which provide CO_2 density as a function of reservoir temperature and pressure for geological storage applications. Reservoir pressure and temperature for each prospect were projected onto the published density chart to estimate in situ CO_2 density under storage conditions.

Brine density was corrected as a function of salinity and in situ pressure-temperature conditions. Geothermal gradients were derived from calibrated bottom-hole temperature (BHT) measurements from key wells within the study area.

3.9. 3D Geocellular Modeling and Structural Characterization

Three-dimensional geocellular models were developed for both selected structures using the Petrel modeling platform. The workflow integrated: (i) structural framework definition and pillar-grid construction; (ii) sedimentological facies modeling; (iii) petrophysical property modeling; and (iv) incorporation of geomechanical properties, including elastic parameters, principal stress fields, and pore-pressure distributions.

4. Results

The results presented in this section summarize the integrated evaluation of the Mugrosa Formation as a potential geological CO_2 storage system within the Middle Magdalena Valley Basin. The analyses combine prospect ranking, seismic interpretation, petrophysical characterization, geocellular modeling, geomechanical assessment, and fault seal evaluation in order to quantify the structural and mechanical integrity of the evaluated prospects. Particular emphasis is placed on understanding the interaction between reservoir heterogeneity, fault behavior, and stress conditions, as these factors collectively control long-term CO_2 containment performance.

4.1. Prospect Ranking and Selection

To prioritize areas with potential for geological CO_2 storage within the Middle Magdalena Valley Basin (MMVB), a multicriteria ranking matrix was applied to 62 candidate prospects previously identified across the basin.

The evaluation criteria were organized according to their relevance to storage security and economic feasibility and included: (i) reservoir thermodynamic conditions, particularly reservoir temperature and pressure, considering that supercritical CO_2 requires temperatures above 31.1 °C and pressures greater than 7.38 MPa; (ii) seal integrity and thickness; (iii) reservoir thickness and petrophysical quality; (iv) burial depth; (v) trap type; (vi) field maturity; and (vii) accessibility and existing infrastructure.

As a result of this assessment, the North Structure and Central Structure emerged as the two highest-ranked prospects, with scores of 41/50 and 40/50, respectively. Both structures are associated with Oligocene Mugrosa Formation reservoirs located at depths compatible with supercritical CO_2 conditions, ranging from 5970 to 6190 ft (1819.7 to 1886.71 m) MD in the North Structure, and from 4245 to 4410 ft (1293.88 to 1344.17 m) and 4600 to 4680 ft (1402.08 to 1426.46 m) MD in the Central Structure.

The selected prospects exhibit favorable structural and stratigraphic conditions for CO_2 storage, including structural closure associated with compressional tectonics, the presence of regionally extensive sealing intervals, and reservoir units with sufficient thickness and injectivity potential. Additionally, their proximity to existing hydrocarbon infrastructure and major CO_2 emission sources enhances their suitability for future CCS implementation scenarios.

4.2. Seismic Interpretation and Structural Geometry

Interpretation of the seismic lines allowed the definition of the structural framework of the study area and the identification of two anticlines within the eastern block, both bounded by reverse faults. These structures exhibit favorable geometric characteristics for geological CO_2 storage, including structural closure, fault-controlled compartmentalization, and the presence of potential sealing intervals associated with fine-grained deposits.

4.2.1. North Structure Prospect

The northern prospect corresponds to an anticline with northwest-southeast vergence and a north-south plunging axis, covering an approximate area of 1.6 km^2 and a width of nearly 2624.67 ft (800 m). The structure is intersected along its eastern crest by a reverse fault associated with the Infantas Fault system, which exhibits compressional kinematics.

Figure 1 shows the interpreted seismic section across the North Structure prospect. The top of the Mugrosa Formation is characterized by high amplitude and laterally continuous reflectors, indicating relatively consistent stratigraphic continuity. In contrast, lower-amplitude and less continuous reflectors were identified toward the upper and basal

sections of the interval, suggesting the presence of shale-rich layers that may act as local sealing units.

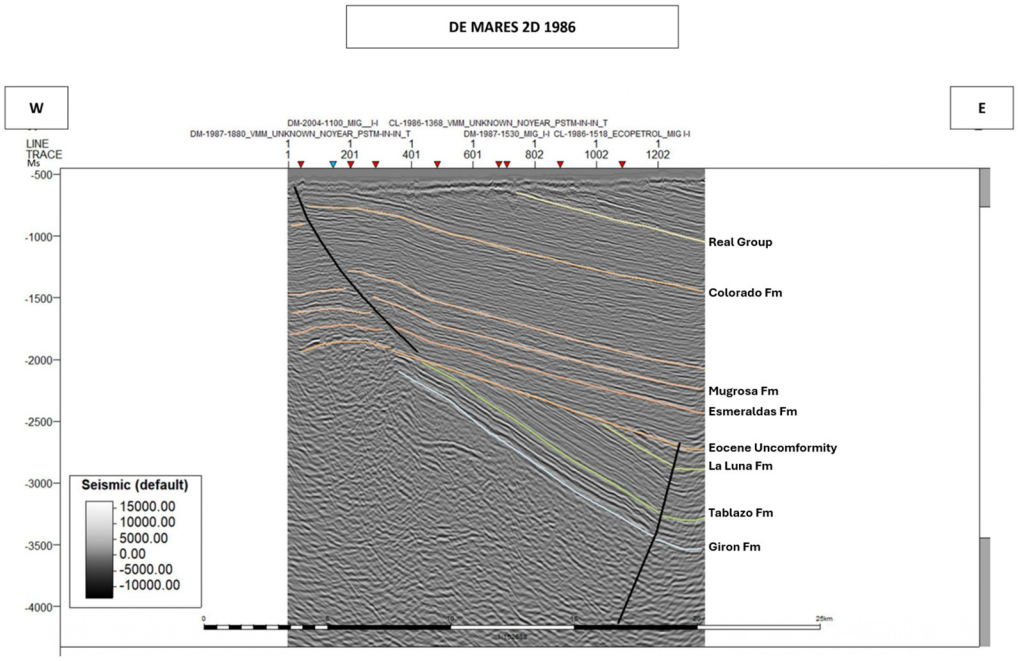


Figure 1. Interpreted 2D seismic section showing the structural configuration of the study area in the Middle Magdalena Valley Basin. Key stratigraphic horizons are highlighted, including the Real, Colorado, Mugrosa, Esmeraldas, Eocene unconformity, La Luna, Tablazo, and Girón formations. The section illustrates a compressional structural regime characterized by a major reverse fault and associated folding, which controls the geometry of the identified anticline structures and potential CO_2 storage traps.

The structural configuration indicates a fault-bounded anticlinal trap with favorable closure conditions for CO_2 accumulation. However, the proximity of the reverse fault to the structural crest suggests that fault integrity and sealing behavior represent critical factors controlling long-term containment performance.

4.2.2. Center Structure Prospect

The Central Structure corresponds to a faulted elongated dome-shaped anticline approximately 2.5 km long and 1.3 km wide, with its principal axis-oriented NW-SE. The fold exhibits a north-south plunging trend and is structurally controlled by compressional deformation associated with reverse faulting.

The structure is bounded to the west by the Arrugas Fault, a high-angle reverse fault dipping eastward and exhibiting northeast vergence. This fault may act as a lateral sealing boundary, contributing to structural closure and compartmentalization within the prospect.

The interpreted seismic geometry suggests the presence of a structurally confined reservoir system characterized by fault-assisted closure and vertical stacking of reservoir-seal intervals (Figure 2). The elongated dome configuration enhances the potential for CO_2 trapping, while the associated reverse fault system may influence both fluid migration pathways and pressure distribution during injection scenarios.

From a storage-integrity perspective, the Central Structure presents favorable geometrical conditions for CO_2 containment; however, the sealing behavior and geomechanical stability of the Arrugas Fault represent key controlling factors that must be evaluated to assess long-term storage security.

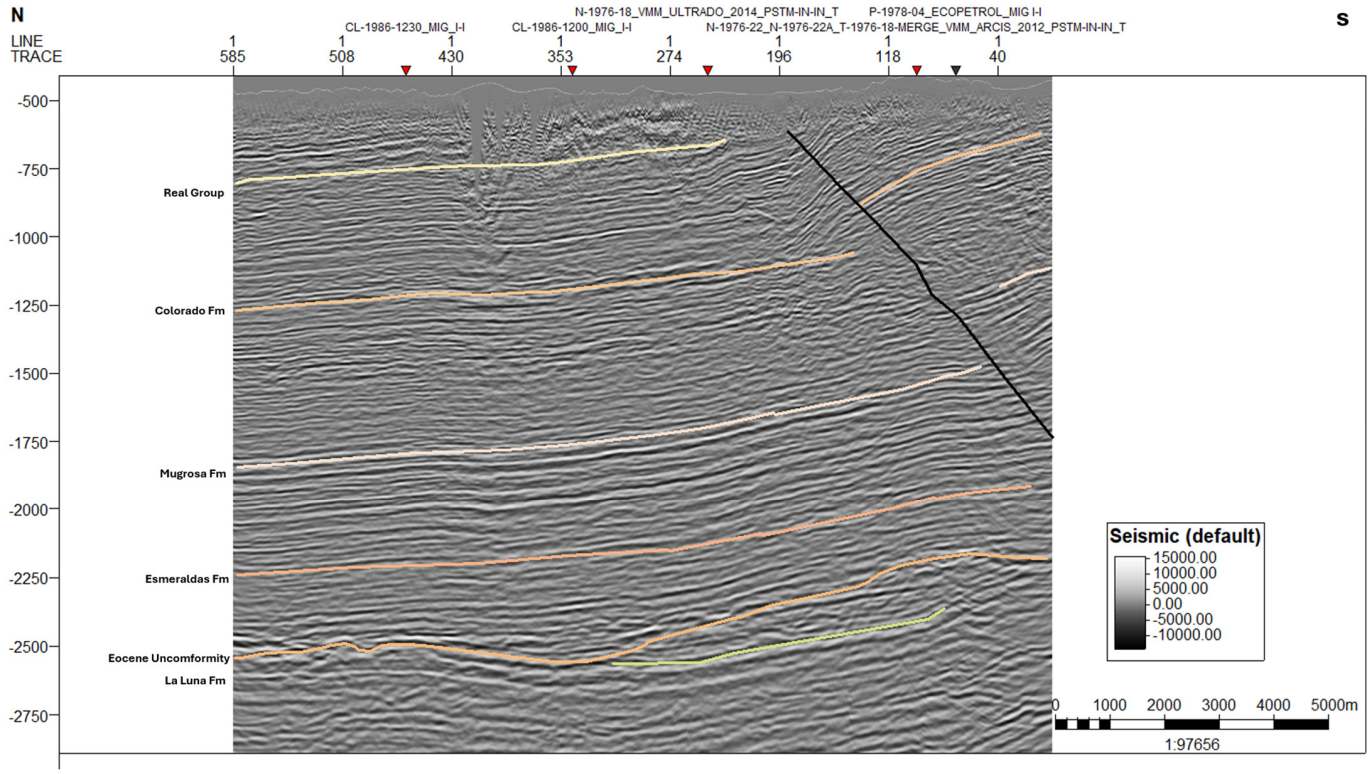


Figure 2. Interpreted 2D seismic section highlighting the structural framework of the study area, including key stratigraphic horizons (Real, Colorado, Mugrosa, Esmeraldas, and the Eocene unconformity). The section shows a reverse fault (black) affecting the stratigraphic sequence and controlling the deformation of overlying units. The geometry reflects a compressional tectonic regime, with gentle folding of the Mugrosa Formation and potential structural trapping conditions relevant for CO_2 storage.

Both structures are interpreted as potential CO_2 storage prospects associated with fault-bounded structural closures developed under compressional tectonics (Figure 3). The Mugrosa Formation constitutes the main storage reservoir due to the presence of laterally continuous sandstone bodies with favorable petrophysical characteristics. In addition, intraformational shale-rich intervals may provide secondary sealing capacity, enhancing vertical containment and contributing to reservoir compartmentalization.

4.3. Petrophysical Analysis of the Mugrosa Formation

The petrophysical evaluation of the Mugrosa Formation involved the integration of well-log data and sedimentological information derived from thin-section analysis using conventional petrophysical interpretation workflows. Thickness distribution reveals significant local-scale variability across the study area, reaching its maximum development in the Margaritas-1 well, where the formation attains approximately 3550 ft (1082.04 m). In contrast, the Marengo-1 and Zarzal-2 wells exhibit comparable thicknesses of 1740 and 1780 ft (530.352 and 542.544 m), respectively, whereas the minimum thicknesses were recorded in the Bambuco-1 (1082 ft, 329.79 m) and Cocodrilo-1 (1501 ft, 457.5 m) wells (Figure 4).

The observed thickness variability reflects the combined influence of synsedimentary accommodation changes, differential subsidence, and structural deformation associated with the tectonic evolution of the basin. These variations directly affect reservoir continuity, storage capacity, and the spatial distribution of petrophysical properties within the geocellular model.

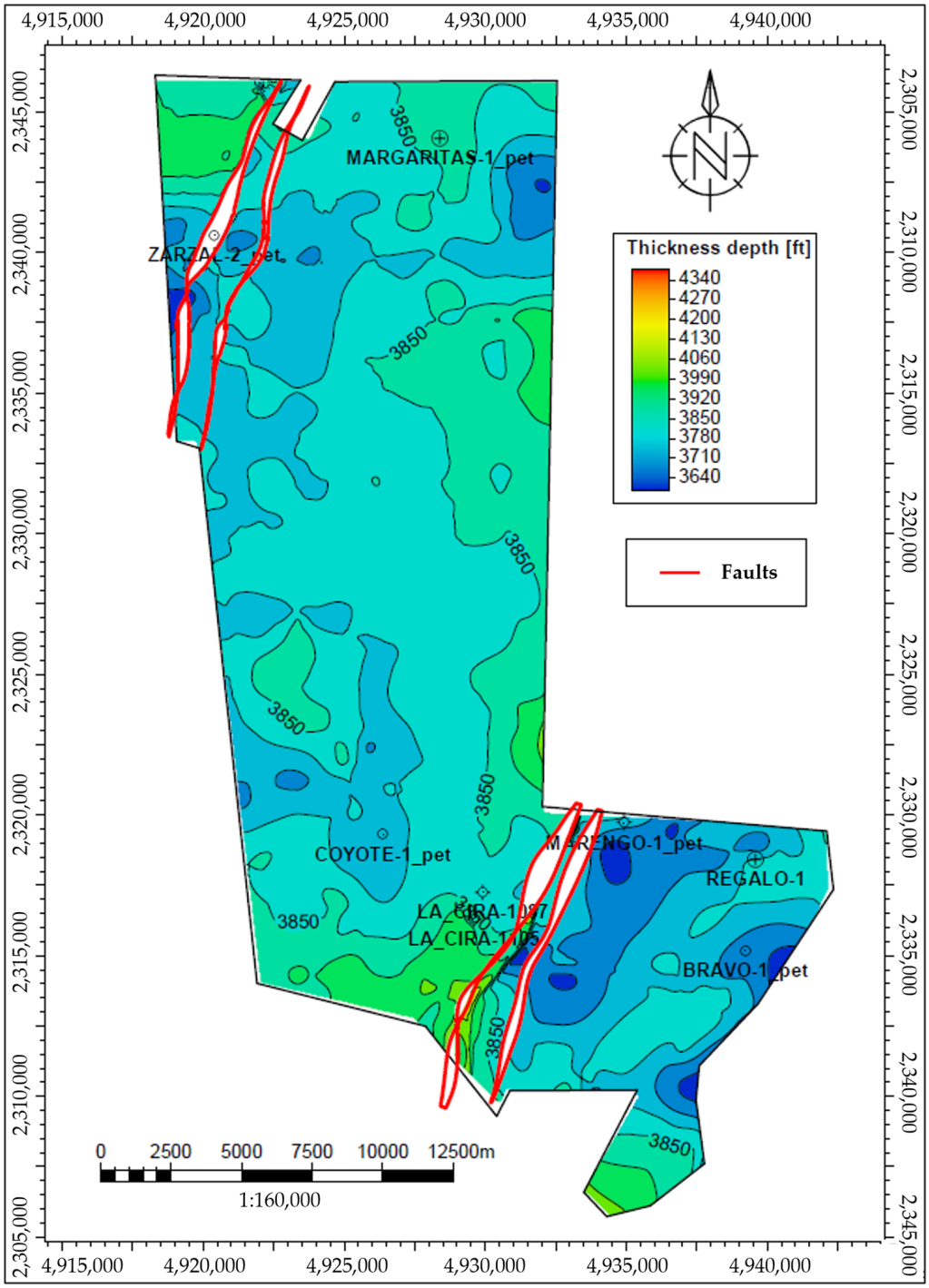


Figure 3. Structural depth map (ft) of the study area showing the spatial distribution of the top of the reservoir and associated fault systems. Contours represent depth variations, highlighting structural lows and highs across the area. Major faults are indicated in red, defining compartmentalization and structural closures relevant for CO_2 storage site for both structures prospect. The locations of key wells (e.g., Margaritas-1, Zarzal-2, Marengo-1, and others) are shown for reference and calibration of the structural model.

The storage quality of the Mugrosa Formation as a potential CO_2 reservoir was evaluated through the analysis of shale volume (*Vsh*), porosity, and permeability derived from petrophysical interpretation. Based on the results obtained, the analyzed wells were differentiated according to their dominant lithological character, defining two main depositional trends: clay-dominated intervals and sandstone-dominated intervals.

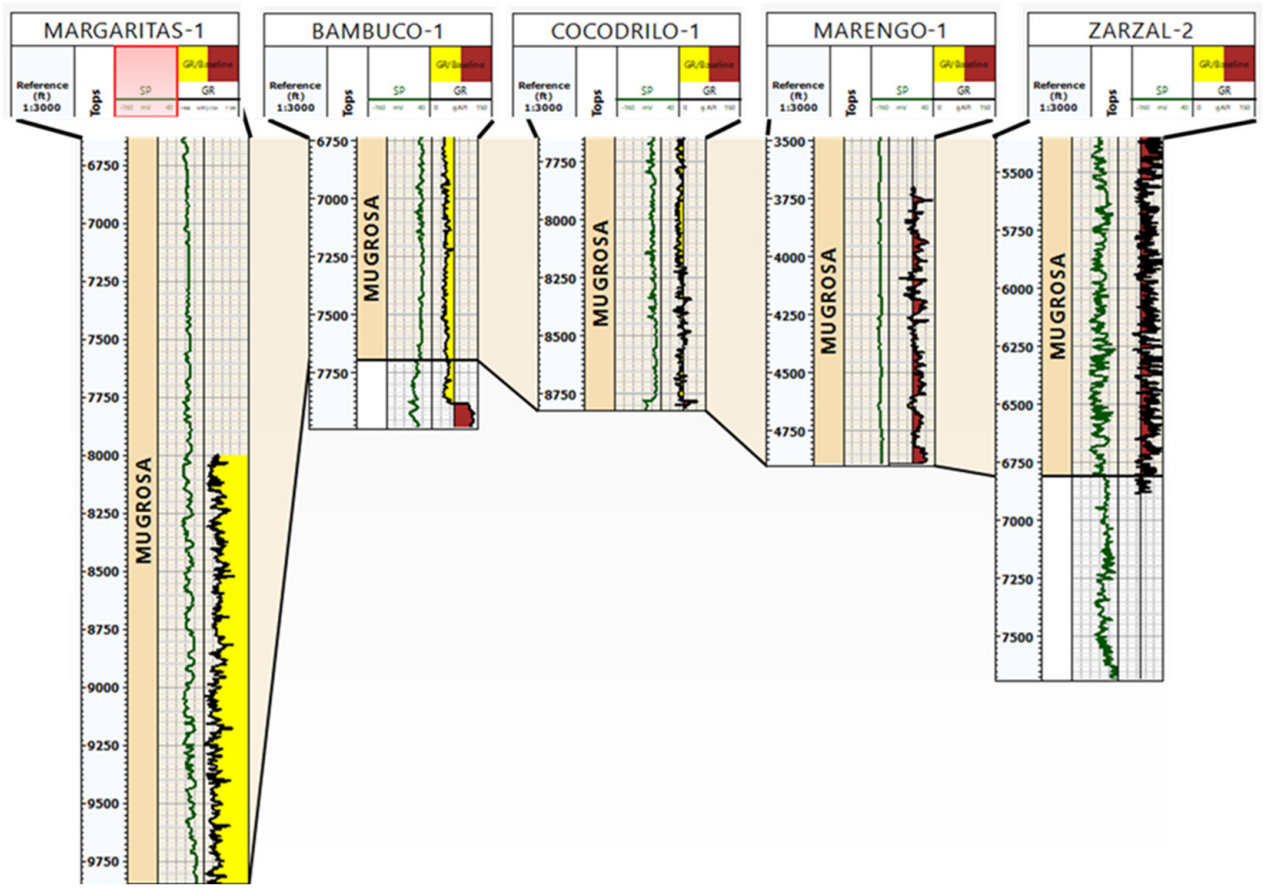


Figure 4. Correlation panel of well logs across the study area (Margaritas-1, Bambuco-1, Cocodrilo-1, Marengo-1, and Zarzal-2) illustrating the vertical and lateral continuity of the Mugrosa Formation. The logs include *GR* and SP, highlighting lithological variability and facies distribution. The correlation shows a predominance of high *GR* values, indicative of clay-rich intervals, with localized lower *GR* zones corresponding to potential sandy interbeds, supporting the interpretation of a heterogeneous reservoir system.

In the Marengo-1 and Zarzal-2 wells, the Mugrosa Formation is characterized by a continuous and relatively homogeneous succession with a clear predominance of shale-rich facies. Gamma ray readings exceed 130 gAPI within the most argillaceous intervals in the Zarzal-2 well, while minimum values near 60 gAPI correspond to the cleanest intervals. A similar behavior was identified in the Marengo-1 well. Based on these responses, calculated *Vsh* values exceed 90% across large portions of the formation, indicating poor overall reservoir quality. Nevertheless, the Zarzal-2 well exhibits a higher frequency of thin interbedded intervals interpreted as sandstone horizons, which may locally improve storage potential (Figure 5).

The predominance of fine-grained facies suggests reduced effective porosity and limited reservoir connectivity over significant portions of the formation. However, discrete sandstone intercalations may provide locally injectable intervals that enhance storage capacity and fluid transmissibility within the otherwise shale-dominated succession.

In contrast, the Cocodrilo-1 and Bambuco-1 wells are dominated by sandstone lithologies (Figure 6). In the Bambuco-1 well, the Mugrosa Formation consists of a relatively monotonous and laterally continuous sandstone succession with low shale content, suggesting more favorable reservoir conditions in terms of storage capacity and injectivity.

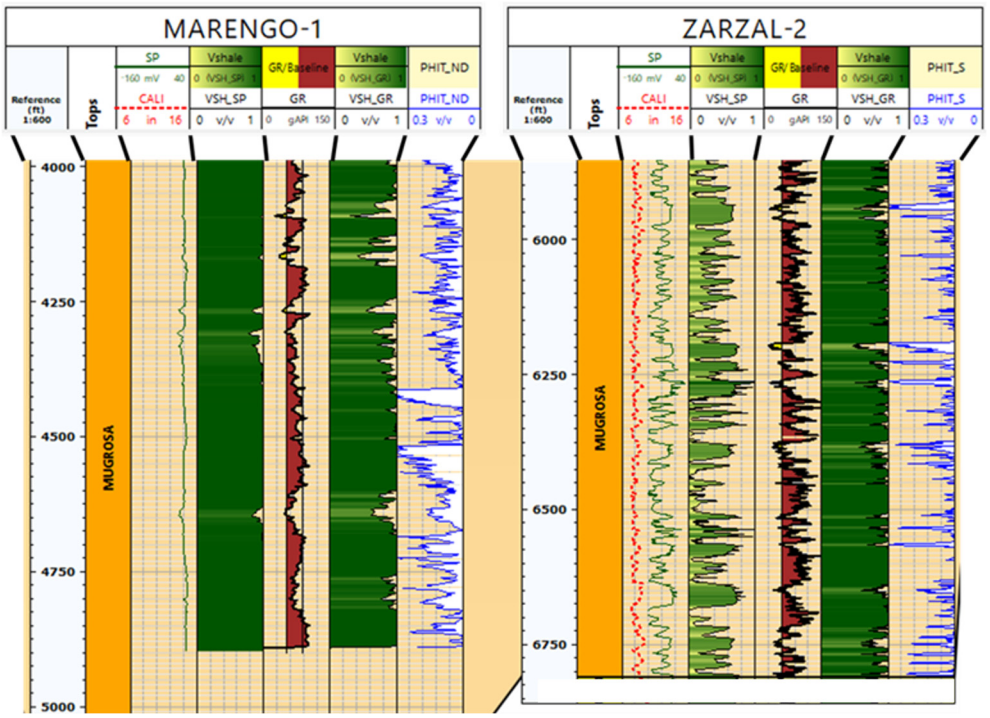


Figure 5. Composite well-log panels for the Marengo-1 and Zarzal-2 wells across the Mugrosa Formation, showing SP, caliper (CALI), *GR*, *Vsh*, and total porosity (PHIT). The logs indicate predominantly shale-rich intervals with limited discrete porous sandy bodies, highlighting lateral heterogeneity in reservoir quality within the studied formation.

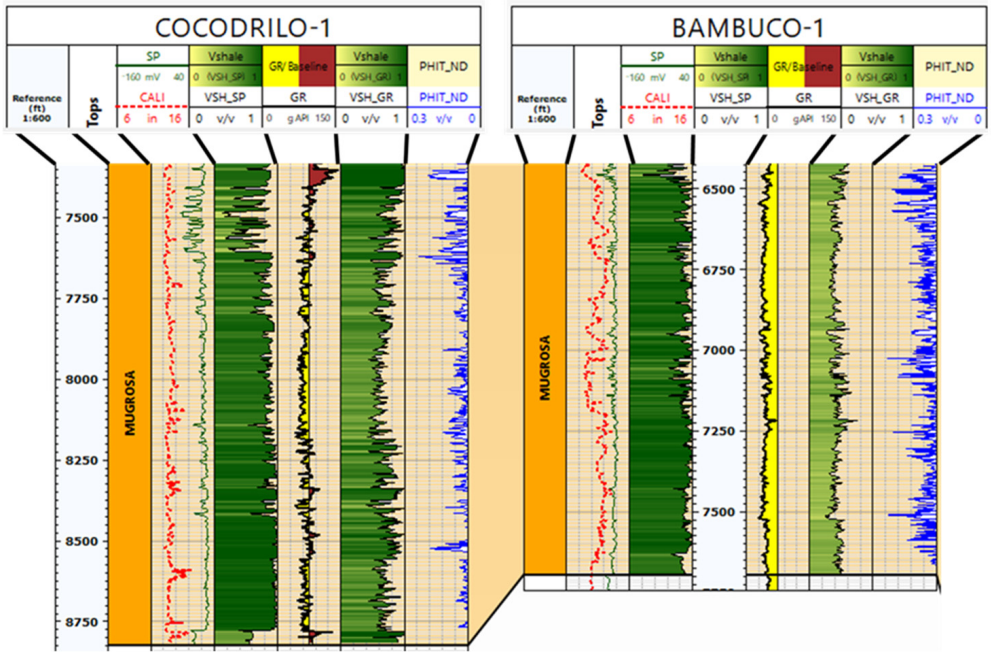


Figure 6. Composite well-log panels for the Cocodrilo-1 and Bambuco-1 wells across the Mugrosa Formation, showing SP, *GR*, Caliper (CALI), *Vsh*, and total porosity (PHIT). The logs reveal predominantly shale-rich intervals with limited porous sandy interbeds, confirming the strong lithological heterogeneity.

Conversely, the Cocodrilo-1 well displays greater internal heterogeneity, characterized by the interbedding of shale intervals with average thicknesses ranging from 20 to 40 ft (6.1 to 12.19 m), particularly toward the upper and basal sections of the formation. This

stratigraphic variability indicates a more compartmentalized reservoir architecture, where alternating sandstone and shale layers may influence vertical connectivity, fluid migration pathways, and pressure distribution during CO_2 injection.

The spatial variability observed among the analyzed wells highlights the strong depositional control on reservoir quality within the Mugrosa Formation. Sandstone-dominated sectors exhibit more favorable petrophysical conditions for CO_2 storage, whereas shale-rich intervals contribute to local sealing capacity and internal stratigraphic compartmentalization.

Sandstone intervals with *Vsh* values ranging between 40% and 50% exhibit relatively low effective porosities, on the order of 10%, and permeabilities ranging from 500 to 800 mD. Despite the comparatively modest porosity and permeability values inferred for the sandstone intervals of the Mugrosa Formation, particularly in the Cocodrilo-1 well, these intervals may still represent viable targets for geological CO_2 storage.

This interpretation is supported by the favorable reservoir-seal configuration identified within the formation, where shale-rich horizons act as effective intraformational seals with considerable thickness and lateral continuity. Such stratigraphic architecture may enhance vertical containment capacity and reduce the risk of upward CO_2 migration during injection operations.

Additionally, well-log analysis did not reveal evidence of hydrocarbon accumulations within the evaluated intervals, allowing the exclusion of enhanced oil recovery (EOR) applications as a primary development strategy and reinforcing the suitability of the formation for dedicated geological CO_2 storage purposes.

The coexistence of moderate-quality sandstone bodies and laterally persistent shale intervals suggest that storage system is controlled by stratigraphic heterogeneity, where storage efficiency and injectivity are strongly influenced by the spatial distribution and connectivity of reservoir facies. Consequently, detailed geocellular representation of these heterogeneities becomes essential for accurately evaluating storage performance and containment integrity.

4.4. Property Modeling

Once reservoir characterization was completed and the geological and petrophysical properties were defined, the construction of the geocellular model was undertaken. This model provides a more accurate representation of the spatial distribution of facies and reservoir properties, thereby facilitating the evaluation of the CO_2 storage potential within the Mugrosa Formation.

Cell-based modeling techniques combined with statistical and anisotropy analyses were applied to reproduce the spatial heterogeneity of the reservoir. The resulting three-dimensional framework captures the variability in lithological distribution, petrophysical properties, and stratigraphic architecture, allowing the identification of preferential flow pathways and potential storage compartments.

The facies model was populated using geostatistical simulation methods constrained by well-log interpretation, sedimentological characterization, and structural geometry. This approach enabled the generation of spatially consistent facies distributions that honor both local well data and regional depositional trends. Subsequently, petrophysical properties including porosity, permeability, and shale volume were distributed within the grid according to the previously defined facies associations.

Anisotropy analysis revealed preferential continuity along the principal depositional directions, particularly within sandstone-dominated intervals interpreted as channelized fluvial deposits. These trends exert control on reservoir connectivity and may significantly influence CO_2 plume migration and pressure propagation during injection scenarios.

The resulting geocellular model constitutes a fundamental component of the integrated workflow, as it provides the structural and petrophysical basis for subsequent geomechanical assessment, fault seal evaluation, and future storage-capacity estimation through dynamic simulation. Moreover, the detailed representation of reservoir heterogeneity is critical for identifying the most favorable intervals for CO_2 injection and long-term containment under secure storage conditions.

4.4.1. Structural Model

The two identified prospects are associated with fault-bounded structural closures developed against reverse faults. The North Structure prospect is controlled by the Infantas Fault, which exhibits a SW-NE strike and an average dip angle of 43°. In contrast, the Central Structure prospect is associated with the Arrugas Fault, characterized by a SW-NE strike and an average dip of 34° (Figure 7).

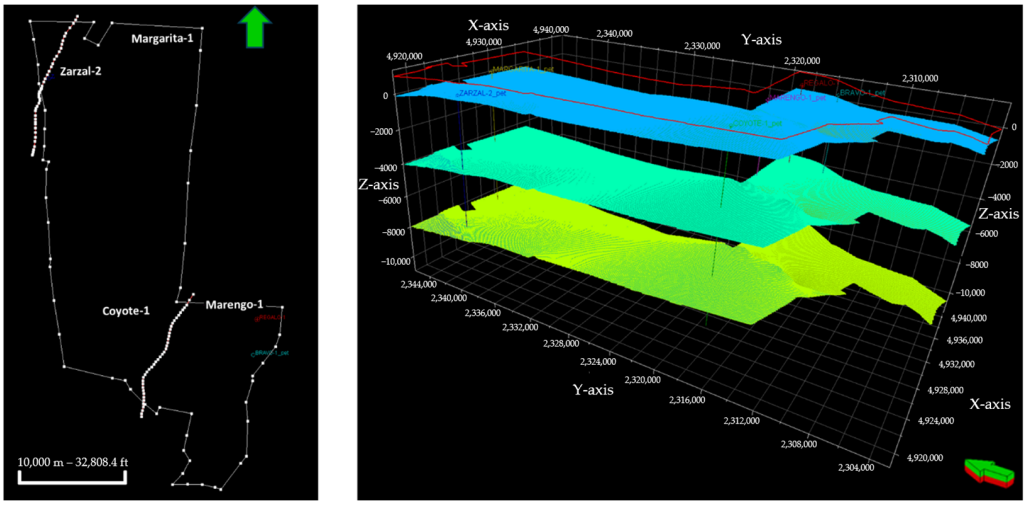


Figure 7. Areal and spatial distribution of wells (**left**) and three-dimensional structural framework of the Mugrosa Formation (**right**), showing the interpreted stratigraphic horizons used to constrain the geocellular model. The structural surfaces define the regional geometry of the storage interval and provide the basis for reservoir zonation, volumetric estimation, and subsequent static modeling.

Both fault systems exert a major control on the structural configuration of the study area, compartmentalizing the reservoir into three principal structural blocks (Figure 8). This compartmentalization influences reservoir continuity, fluid communication, and pressure distribution, representing a key factor in the evaluation of CO_2 migration and containment behavior.

4.4.2. Facies Model

The facies model reproduces the spatial heterogeneity of the reservoir and includes multiple stochastic realizations designed to capture the inherent geological uncertainty of the system (Figure 9). These realizations provide a probabilistic representation of facies distribution and are essential for evaluating the influence of sedimentary variability on petrophysical properties and fluid-flow behavior within the static model.

The simulated facies architecture highlights the spatial distribution and connectivity of sandstone and shale bodies, allowing the identification of preferential storage intervals and potential intraformational barriers. This heterogeneity suggests direct control on reservoir connectivity, injectivity, and the spatial evolution of the CO_2 plume during injection scenarios.

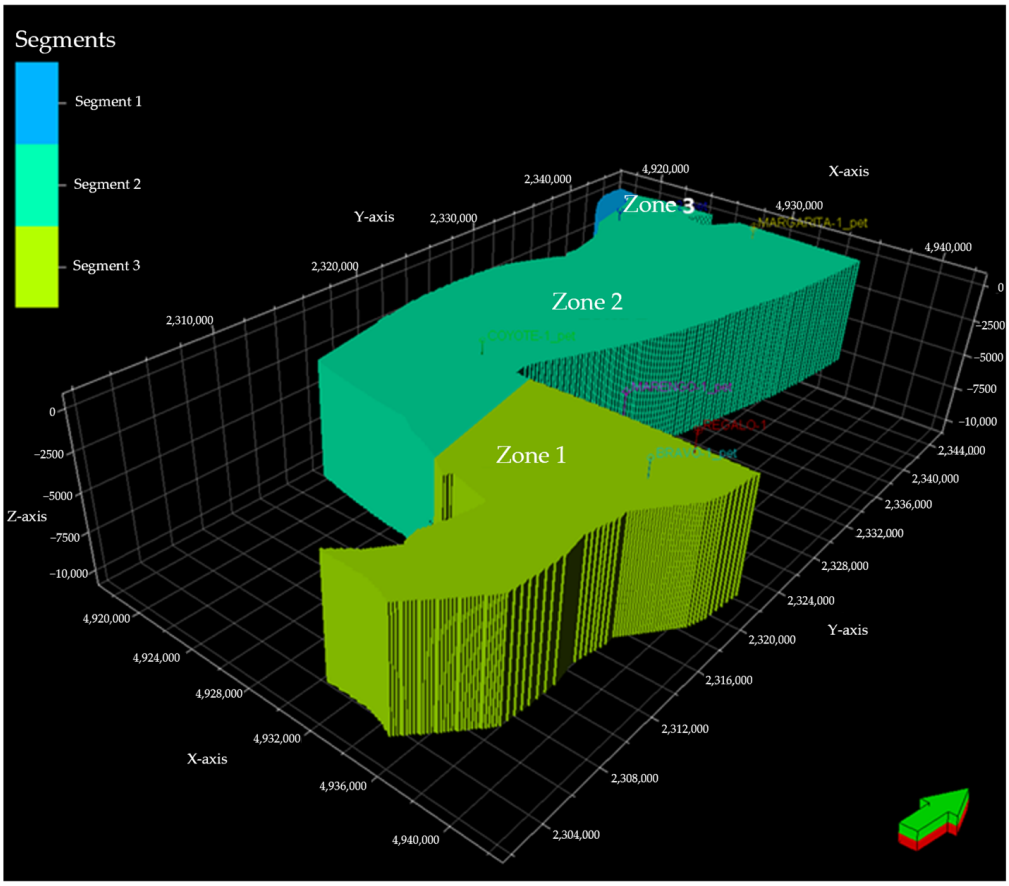


Figure 8. Structural segmentation of the 3D geocellular model into three segments (Zone 1, Zone 2, and Zone 3), highlighting reservoir compartmentalization and its implications for fluid flow and CO_2 storage.

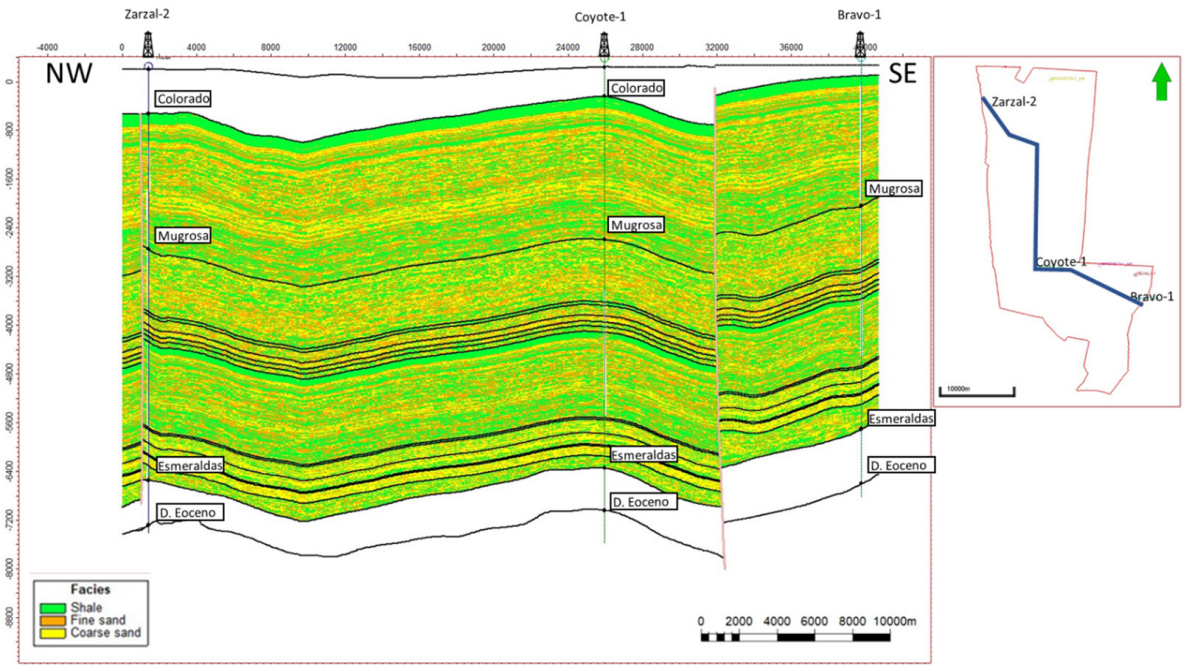


Figure 9. Stratigraphic cross-section (NW-SE) showing facies distribution and formation tops (Colorado, Mugrosa, Esmeraldas, and Oligocene), illustrating vertical heterogeneity and depositional architecture. The inset map (right) indicates the well correlation panel location.

4.4.3. Petrophysical Model

Petrophysical property modeling allowed the distribution of porosity, permeability, and water saturation within the geocellular model while honoring the upscaled values derived from well-controlled cells.

Within the Mugrosa Formation reservoirs, intervals with average effective porosity values close to 15% were identified in the Central prospect, particularly between 4245–4410 ft (1293.876–1344.168 m) and 4600–4680 ft (1402.08–1426.46 m). In the North prospect, average effective porosity values range between 13% and 14% within the 5970–6190 ft (1819.656–1886.71 m) and 6403–6565 ft (1951.63–2001.01 m) intervals (Figure 10A). These results are consistent with values reported from producing reservoirs in nearby fields, supporting the reliability of the petrophysical interpretation and reducing uncertainty associated with modeling.

The modeled permeability distribution within the Mugrosa reservoirs ranges from 500 to 800 mD, consistent with channel-deposit facies interpreted as the dominant depositional environment of the formation (Figure 10B). These permeability values indicate favorable pore connectivity within the reservoir intervals, enhancing fluid transmissibility and supporting the injectivity requirements for geological CO_2 storage.

In contrast, the intervals of sealing facies associated with reservoirs units exhibit permeability ranging from 0.01 to 0.1 mD, characteristic of shale-rich floodplain and overbank deposits. These fine-grained intervals behave as intraformational baffle zones that reduce vertical transmissibility and contribute to the stratigraphic compartmentalization of the reservoir. Their spatial continuity and relatively lower permeability may locally retard upward CO_2 migration, thereby enhancing containment efficiency within the identified storage intervals.

The spatial distribution of petrophysical properties highlights the strong control exerted by depositional facies on reservoir quality and storage performance. Sandstone-dominated intervals exhibit the most favorable injectivity conditions, whereas shale-rich facies contribute to internal compartmentalization and enhanced containment efficiency.

4.5. Geomechanical Model

The integration of geomechanical properties into the geocellular model enabled the evaluation of the spatial relationship between mechanical behavior and the lithofacies architecture previously defined within the reservoir. Statistical analyses and property histograms revealed systematic variations among facies with respect to Young's modulus, cohesion, pore pressure, and fault reactivation potential (Figure 11).

The results indicate a relationship between geomechanical properties and sedimentological characteristics, confirming that facies distribution exerts a significant control on the mechanical response of both reservoir and sealing intervals. Sandstone-dominated facies (reservoirs) generally exhibit higher Young's modulus values, indicating greater elastic rigidity, whereas shale-rich facies (seal) tend to display comparatively lower stiffness and more homogeneous mechanical behavior. Cohesion distributions also reveal facies-dependent variability, with cohesion values generally increasing with sandstone content. However, the highest cohesion values were identified in dirty sandstone intervals, likely associated with mixed sandy-argillaceous compositions and increased matrix support.

Pore-pressure distributions remain relatively consistent across facies, although localized variations may reflect compartmentalization effects associated with structural discontinuities and facies architecture. In general, pore pressure tends to decrease within sandstone-rich facies and increase in finer-grained lithologies, reflecting the lower permeability and greater fluid-retention capacity of shale-rich intervals.

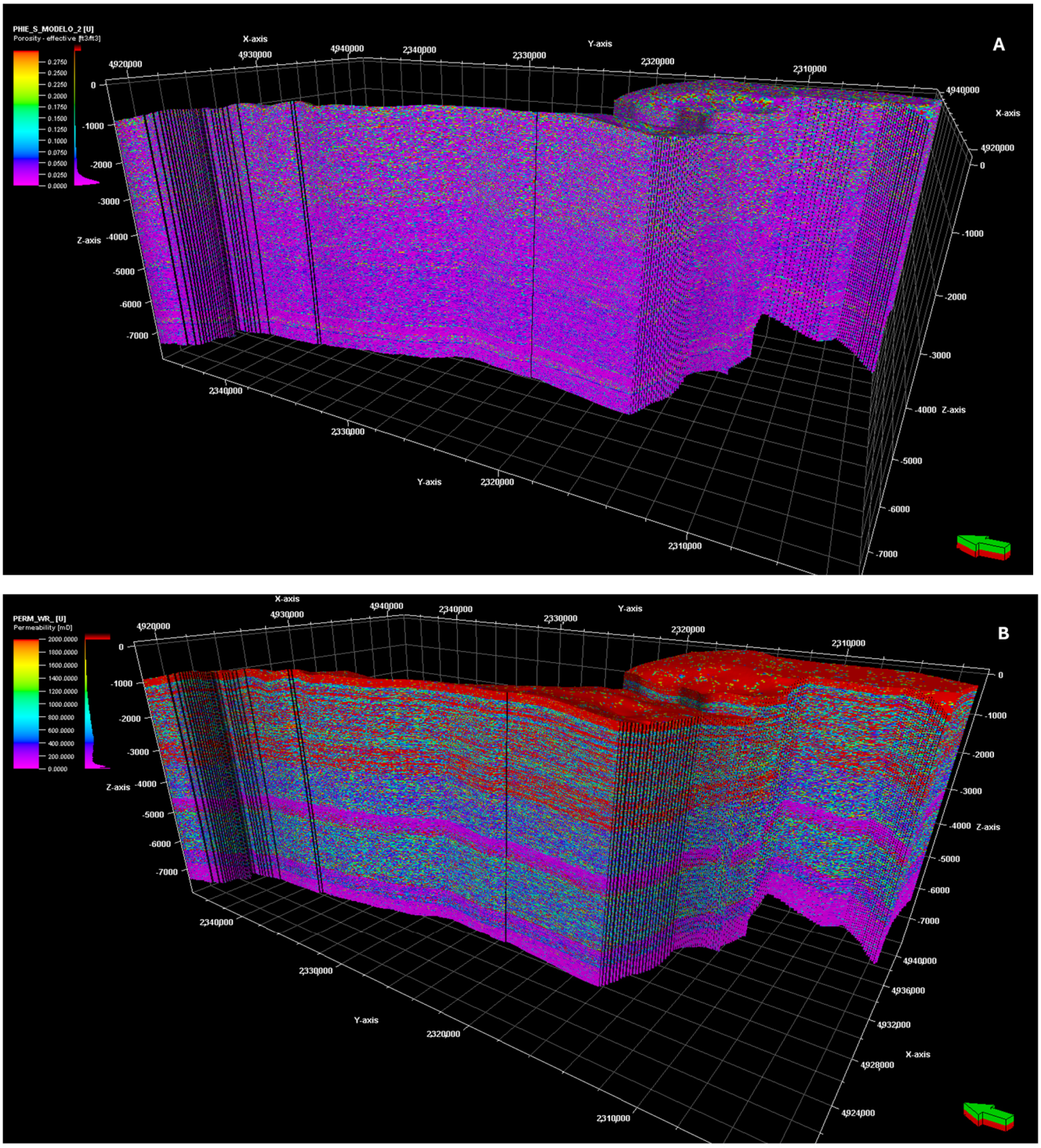


Figure 10. Three-dimensional geocellular model illustrating petrophysical properties: (**A**) effective porosity (v/v); (**B**) permeability (mD), evidencing vertical and lateral heterogeneity.

Similarly, the fault stability parameter exhibits moderate variability among lithologies, indicating that mechanical contrasts within the reservoir may influence stress redistribution and fault reactivation susceptibility during CO_2 injection. The results further suggest that slip susceptibility increases in intervals with higher claystone content, implying that mechanically weaker and more ductile facies may be more sensitive to stress perturbations induced by injection-related pressure changes.

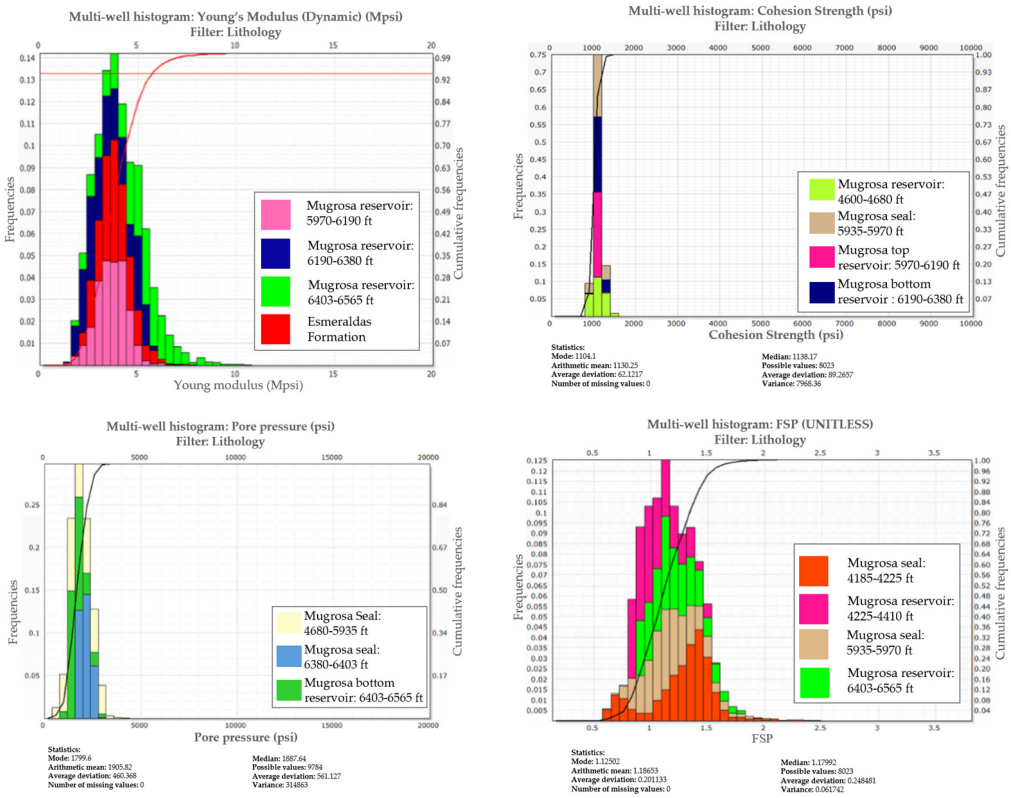


Figure 11. Statistical distributions of geomechanical properties within the geocellular model, including Young's modulus, cohesion strength, pore pressure, and fault stability parameter as a function of lithofacies. The histograms illustrate the influence of sedimentological heterogeneity on the mechanical behavior and stability conditions of the reservoir-seal system. The red and black lines indicate the cumulative frequency distribution.

This mechanical heterogeneity is particularly relevant for CO_2 storage applications because it influences pressure propagation, deformation behavior, and the spatial distribution of stress during the CO_2 injection. The incorporation of geomechanical properties within the geocellular framework therefore improves the representation of coupled sedimentological-mechanical reservoir behavior and provides a more robust basis for evaluating subsurface integrity under injection scenarios.

4.5.1. Principal Stresses

The estimated principal stress distributions reveal moderate spatial variability between the North and Central Structures, primarily associated with differences in burial depth and structural position within the study area (Figure 12).

In the North Structure, the vertical stress (σv) at the base of the deepest reservoir interval, between 6500 and 6600 ft (1981.2 and 2011.68 m), was estimated at approximately 5900 psi (40.679 MPa). Similarly, in the area surrounding the Coyote-1 well, vertical stress values range between 5900 and 6100 psi (40.679 and 42.058 MPa) at depths close to 6100 ft (1859.28 m). These relatively higher stress magnitudes are consistent with the greater burial depth and structural loading conditions observed in the northern sector of the model.

In the Central Structure, lower vertical stress magnitudes were identified due to the comparatively shallower reservoir depths. Near the Regalo-1 well, vertical stress values range from 4100 to 4300 psi (28.2685 to 29.647456 MPa) at a depth of approximately 3900 ft (1188.72 m), whereas in the Bravo-1 well area, estimated vertical stresses vary between 4000 and 4200 psi (27.579029 and 28.957981 MPa) at depths close to 3400 ft (1036.32 m).

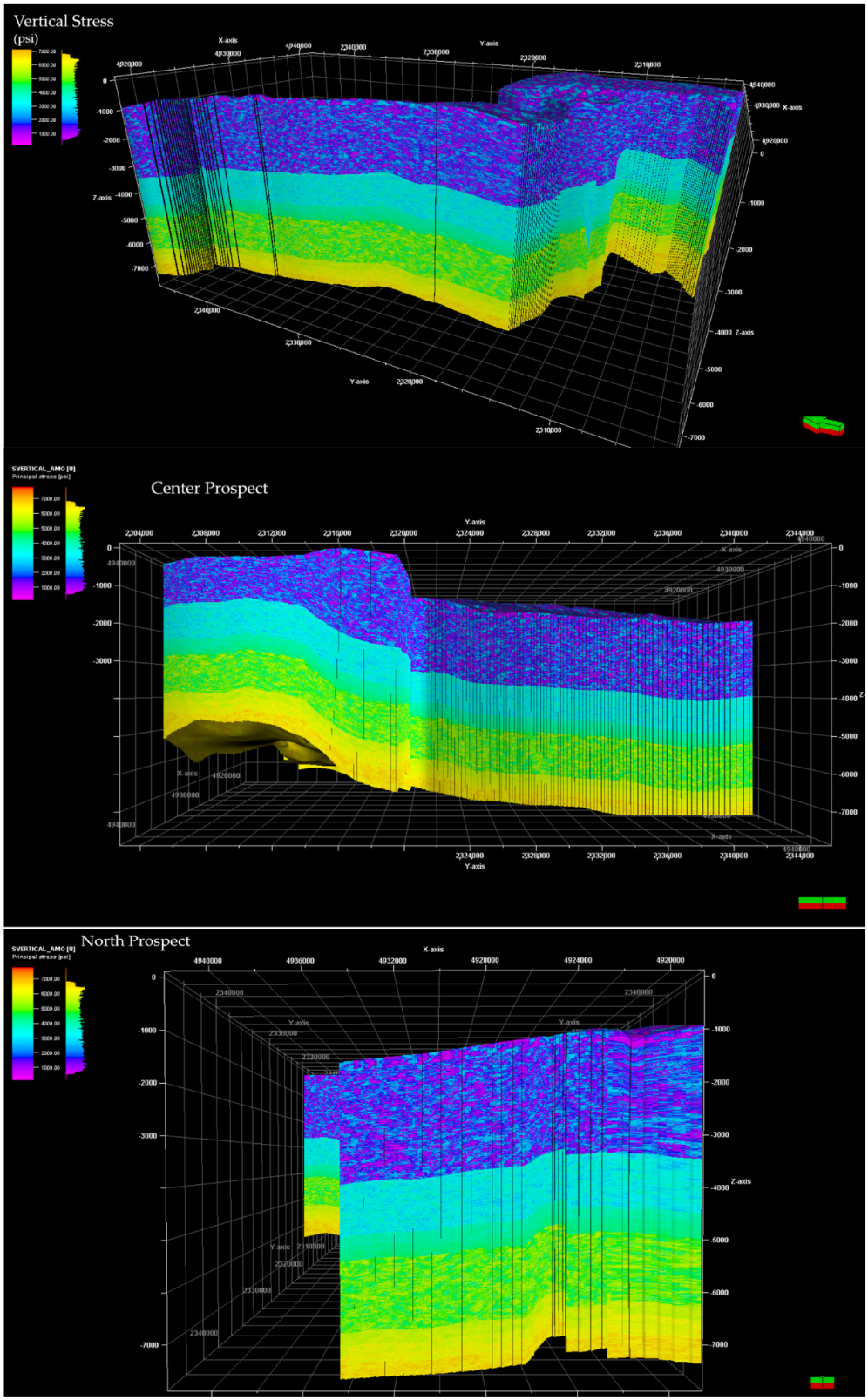


Figure 12. Three-dimensional distribution of vertical stress (σv) within the geocellular model for the North and Central prospects. The model illustrates the increase in vertical stress with burial depth and highlights spatial variations associated with structural configuration and reservoir geometry. Cross-sectional views for both prospects show the stratigraphic distribution of stress magnitudes across the reservoir-seal system, providing a basis for evaluating injection pressure limits and geomechanical stability during CO_2 storage operations.

The observed stress distribution indicates that reservoir depth exerts first-order control on the magnitude of the vertical stress field across the study area. These variations are particularly relevant for defining safe injection pressure windows and evaluating fault stability under CO_2 injection scenarios, as deeper sectors may tolerate higher pore-pressure increases before approaching critical stress conditions.

The minimum (SHmin) and maximum (SHmax) horizontal stresses were estimated using the elastic parameters derived from the geomechanical characterization of the reservoir and sealing units (Figure 13). These calculations incorporated elastic properties obtained from well-log-derived mechanical models, allowing the spatial population of horizontal stresses within the 3D geocellular framework.

For the North Structure, the minimum horizontal stress (SHmin) was calibrated using data from the Zarzal-2 well. The populated model indicates SHmin values ranging from 4600 to 4800 psi (31.71 to 33.09 MPa) at depths between 6300 and 6500 ft (1920.24 and 1981.2 m). Similarly, in the vicinity of the Coyote-1 well, SHmin values between 4800 and 5000 psi (33.09 and 34.47 MPa) were estimated at a depth of approximately 6100 ft (1859.28 m).

In the Central Structure, lower SHmin magnitudes were identified due to the shallower burial conditions. Near the Bravo-1 well, the minimum horizontal stress was estimated at approximately 3500 psi (24.13 MPa) at a depth of 3500 ft (1066.8 m), whereas values between 3600 and 3900 psi (24.821126 and 26.889 MPa) were calculated near the Regalo-1 well at similar depths.

The maximum horizontal stress (SHmax) was estimated for all wells assuming a regional stress orientation of N35°E, consistent with previous tectonic studies of the MMVB and the dominant northeast-southwest compressional regime. In the North Structure, SHmax reaches approximately 6200 psi (42.747 MPa) at depths close to 4600 ft (1402.08 m). In contrast, the Central Structure exhibits SHmax values ranging between 5500 and 5900 psi (37.921165 and 40.679 MPa) near the Bravo-1 well at a depth of approximately 2400 ft (731.52 m), while values between 5000 and 5300 psi (34.474 and 36.54 MPa) were estimated near the Regalo-1 well at a depth of approximately 3900 ft (1188.72 m).

The modeled horizontal stress distribution reflects the combined influence of burial depth, structural configuration, and regional tectonic stress orientation. These results are particularly relevant for defining fracture gradients, evaluating fault stability, and constraining operational injection pressures under CO_2 storage conditions.

4.5.2. Pore Pressure

Pore pressure was estimated using the Eaton method, integrating both sonic and resistivity logs to improve the reliability of the pressure prediction model. This approach enabled the generation of pore-pressure profiles for each well and the identification of intervals where abnormal pressure conditions could potentially compromise formation stability.

The populated geomechanical model indicates that, within the North Structure, pore pressure calibrated with the Zarzal-2 well ranges between 8 and 9 ppg at reservoir depths close to 5000 ft (1524 m). Similarly, in the Coyote-1 well area, pore-pressure values between 8 and 9 ppg were estimated at a depth of approximately 4800 ft (1463.04 m).

For the Central Structure, pore pressure calibrated using the Regalo-1 well, range between 8.6 and 8.8 ppg at depths close to 4500 ft (1371.6 m). In the Bravo-1 well, pore-pressure values between 8.6 and 8.9 ppg were estimated at a depth of approximately 4000 ft (1219.2 m). These intervals correspond to the main reservoir sections identified within the Mugrosa Formation (Figure 14).

Overall, the modeled pore-pressure distribution suggests relatively stable pressure conditions across both prospects, with no evidence of significant overpressure development within the evaluated reservoir intervals. These conditions are favorable for CO_2 storage

operations, as they reduce the likelihood of injection-induced fracturing and contribute to maintaining mechanical stability during pressure buildup.

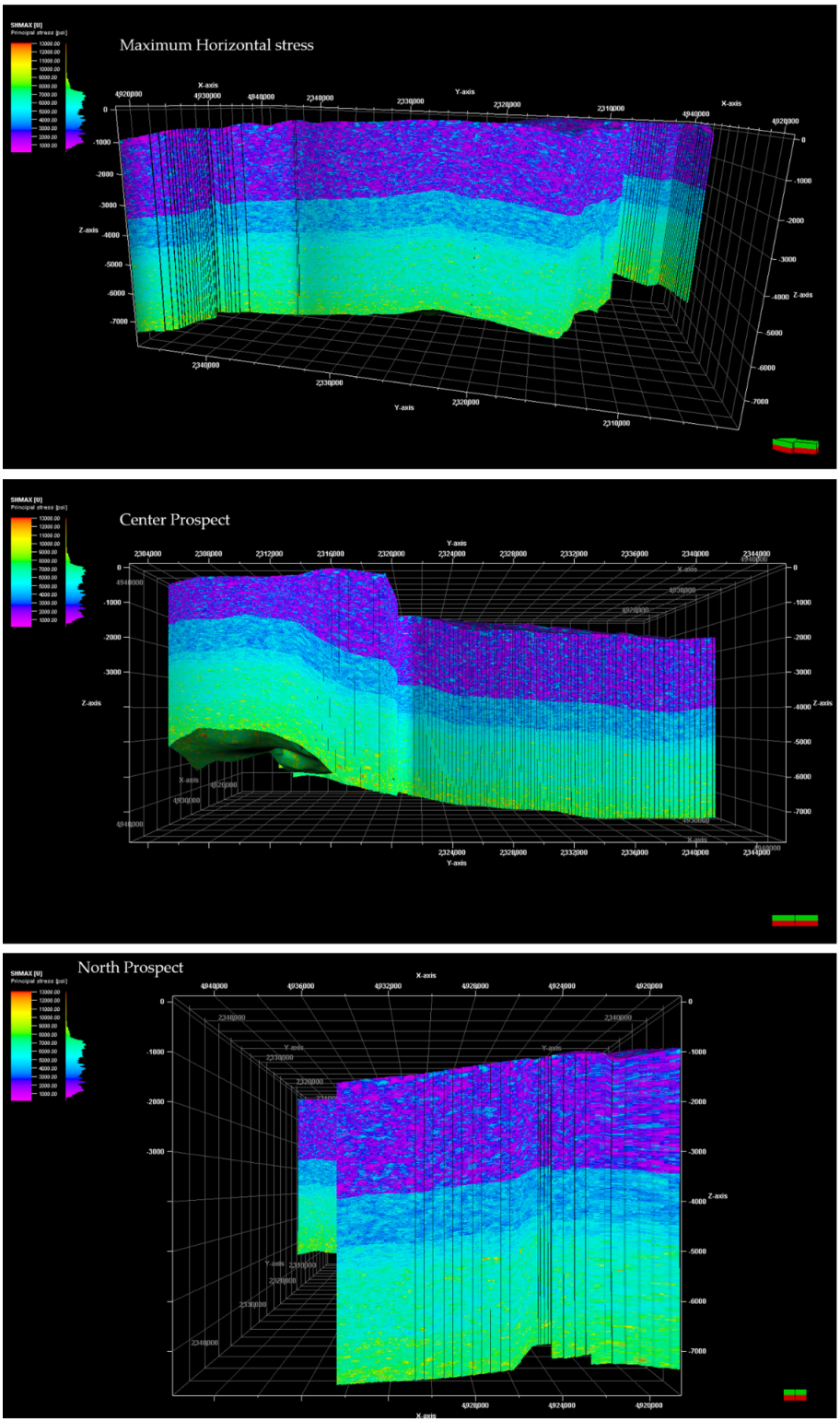


Figure 13. Three-dimensional distribution of maximum horizontal stress (SHmax) within the geocellular model for the North and Central prospects. The populated stress model illustrates the spatial variability of horizontal stress magnitudes associated with structural geometry, burial depth, and regional tectonic orientation. Cross-sectional views highlight the stress distribution across the reservoir-seal system and provide a framework for evaluating fracture propagation and fault reactivation potential during CO_2 injection.

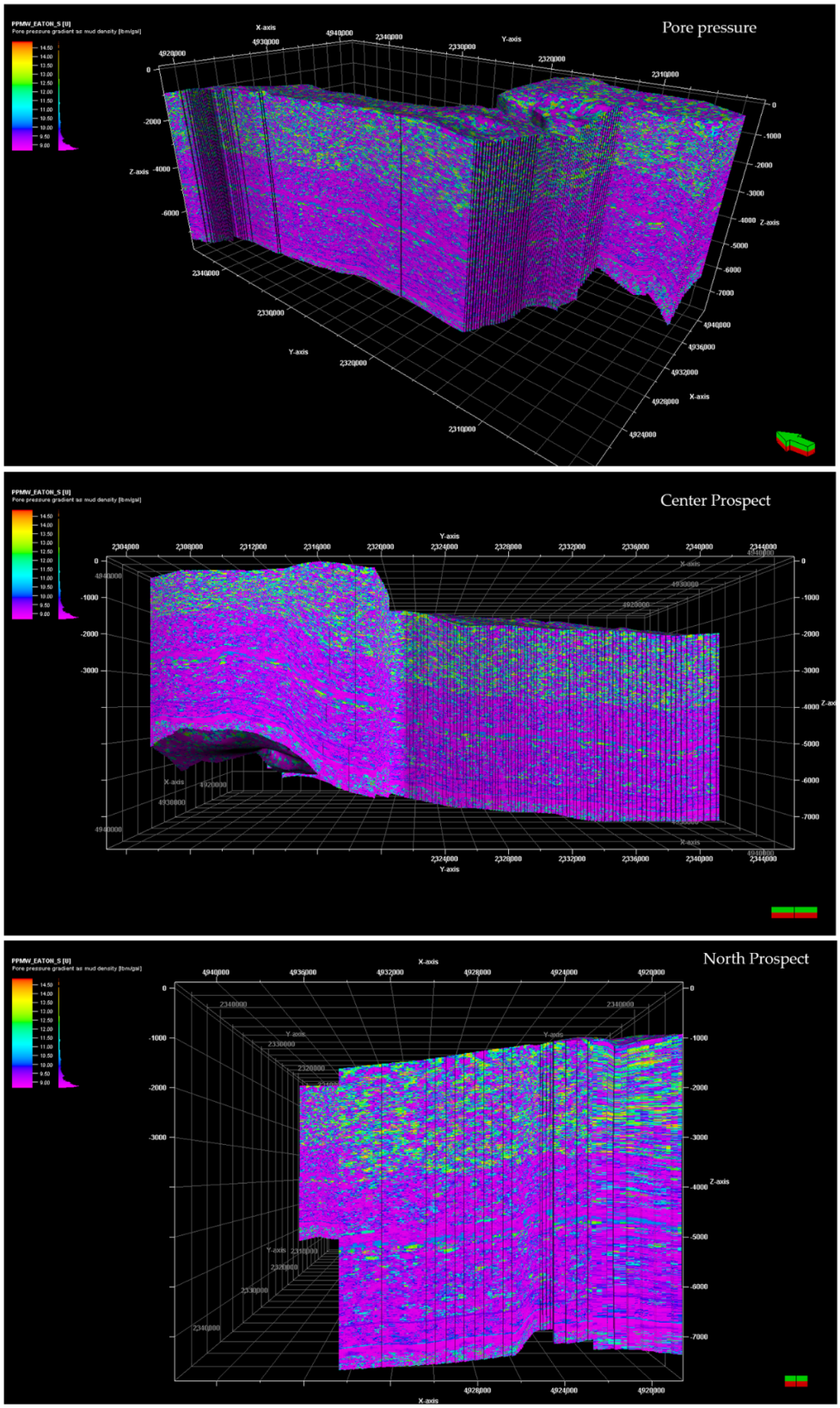


Figure 14. Three-dimensional pore-pressure distribution within the geocellular model for the North and Central prospects. The populated model illustrates the spatial variability of pore pressure across the reservoir-seal system, calibrated using well-log derived Eaton pressure predictions. Cross-sectional views highlight pressure trends within the Mugrosa Formation and provide a basis for evaluating injection safety limits and geomechanical stability during CO_2 storage operations.

4.5.3. Mechanical Properties

According to the geomechanical modeling results, the mechanical properties of the rock units were estimated using P-wave velocity and density log data. Young's modulus and Poisson's ratio were calculated as key elastic parameters controlling rock stiffness and deformation behavior under stress conditions. These properties were subsequently incorporated into the geocellular model to evaluate the capacity of the reservoir-seal system to withstand stress changes induced by CO_2 injection.

The calculated Young's modulus values reflect the elastic rigidity of the formations, whereas Poisson's ratio describes the relationship between axial and lateral deformation under mechanical loading. The spatial distribution of these parameters provides important constraints for assessing deformation potential, fracture susceptibility, and seal integrity during injection scenarios.

The populated Young's modulus model shows a general increase in stiffness with depth, indicating that deeper intervals tend to exhibit greater resistance to deformation under stress conditions (Figure 15). In the North Structure, seal intervals display Young's modulus values ranging between 1.8 and 3.4 Mpsi (12.41 and 23.44 GPa), which are consistent with typical claystone-dominated lithologies. Values approaching 3.4 Mpsi (23.44 GPa) suggest relatively compact and mechanically competent sealing units, potentially reducing deformation susceptibility and improving containment efficiency against upward CO_2 migration.

In the Central Structure, Young's modulus values range between 2.8 and 3.6 Mpsi (19.31 and 24.82 GPa), indicating comparatively stiffer sealing intervals than those identified in the North Structure. These higher elastic moduli suggest improved mechanical integrity and a greater capacity to withstand pressure perturbations associated with injection operations.

Overall, the modeled elastic properties indicate that both prospects exhibit mechanically competent sealing intervals capable of supporting moderate injection-induced stress increases, although the Central Structure appears to present comparatively more favorable geomechanical conditions for long-term CO_2 containment.

On the other hand, the incorporation of Poisson's ratio into the 3D geocellular model (Figure 16) provides additional constraints for evaluating the mechanical stability of both the reservoir and sealing units under CO_2 injection conditions. In the East Block, the sealing intervals identified in both the North and Central Structures exhibit Poisson's ratio values greater than 0.30, which are characteristic of relatively ductile lithologies with higher lateral deformation capacity. These mechanical characteristics favor stress redistribution and contribute to improved sealing behavior, reducing the potential for upward CO_2 migration into overlying formations.

In contrast, the reservoir intervals display average Poisson's ratio values close to 0.24, indicating an intermediate mechanical behavior between brittle and ductile responses. Although these values suggest mechanically stable reservoir conditions, they also indicate that the reservoir units may become more susceptible to fracturing if injection pressures exceed the operational geomechanical limits defined for the system.

Overall, the combined distribution of Young's modulus and Poisson's ratio indicates a mechanically favorable reservoir-seal configuration, where relatively stiff yet ductile sealing units overlie reservoir intervals with sufficient deformability to accommodate moderate pressure increases during CO_2 injection operations.

4.6. Thermodynamic Conditions and Maximum CO_2 Column Height

The pressure-temperature conditions determined for both evaluated structures indicate that injected CO_2 would remain under dense supercritical conditions, as reservoir tem-

peratures and pressures exceed the critical point of CO_2 (31.1 °C and 1070.4 psi–7.38 MPa). Under these conditions, CO_2 exhibits significantly higher density than in the gaseous phase, improving storage efficiency by increasing the mass of CO_2 stored per unit pore volume while reducing buoyancy effects.

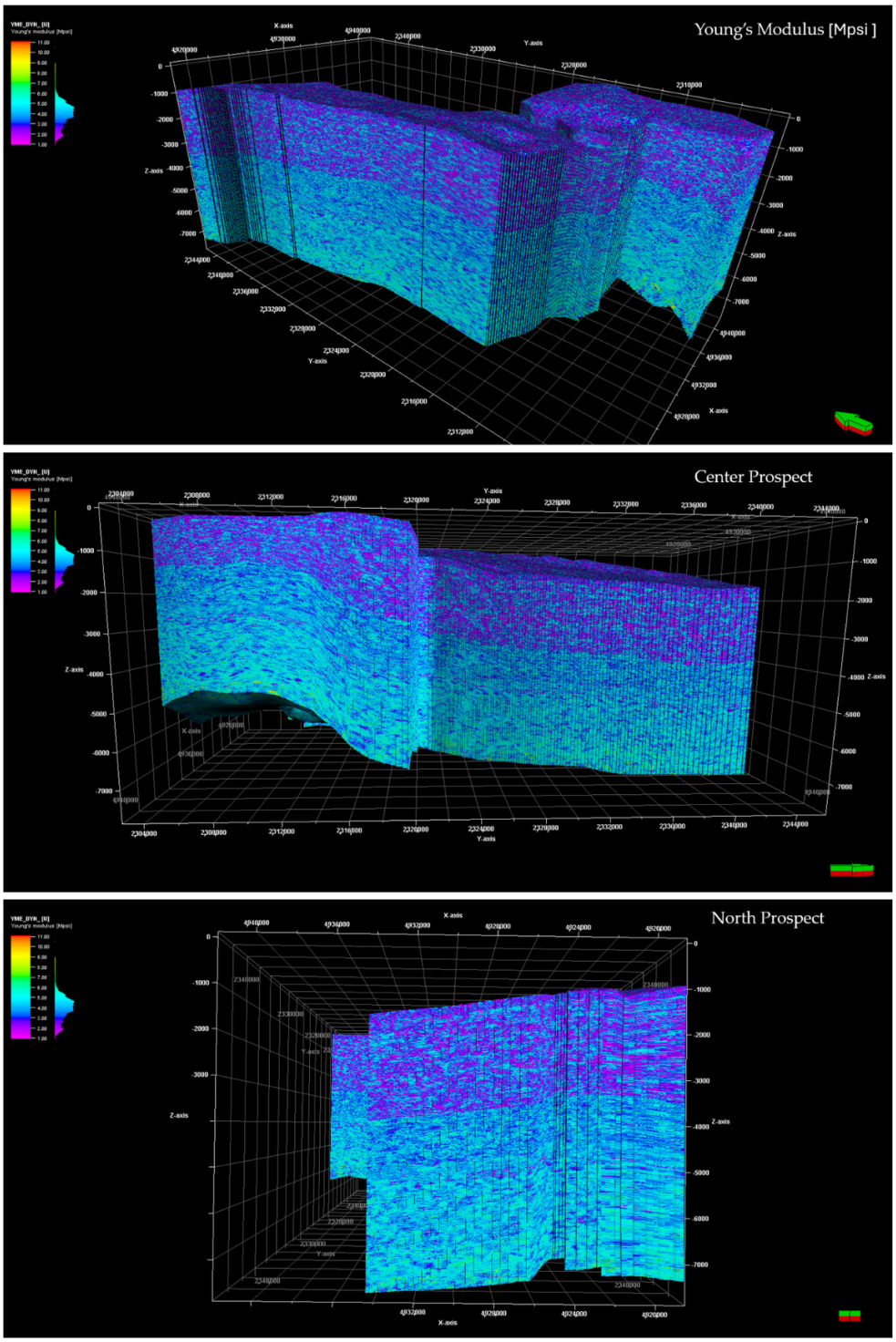


Figure 15. Three-dimensional distribution of Young's modulus within the geocellular model for the North and Central prospects. The populated model illustrates the spatial variability of elastic rigidity across the reservoir-seal system, highlighting the increase in mechanical stiffness with depth and the distribution of mechanically competent sealing intervals relevant for CO_2 containment integrity.

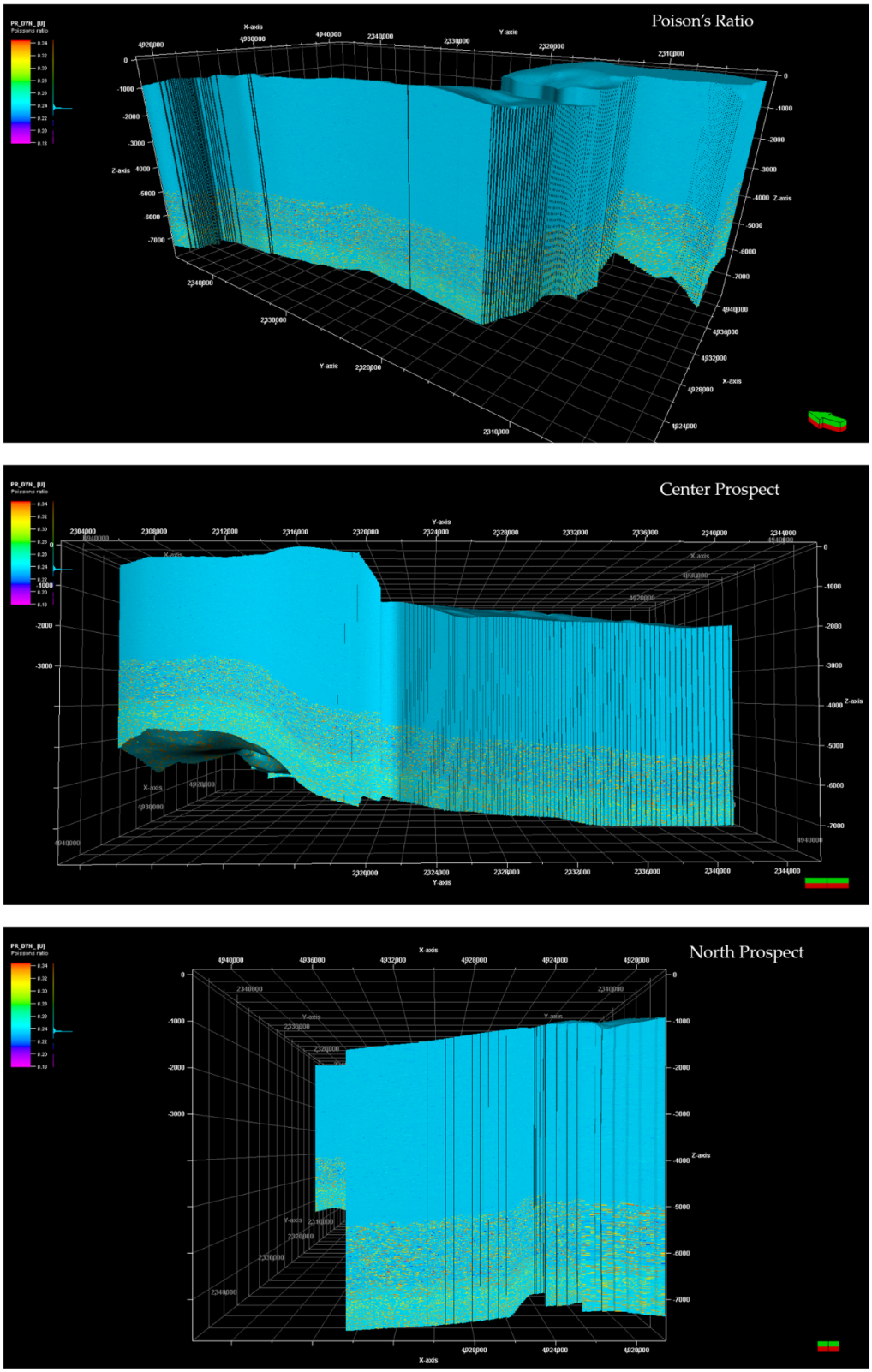


Figure 16. Three-dimensional distribution of Poisson's ratio within the geocellular model for the North and Central prospects. The model highlights the spatial variability of elastic deformation behavior across the reservoir-seal system, illustrating the presence of relatively ductile sealing intervals and mechanically stable reservoir units relevant for evaluating CO_2 containment integrity and fracture susceptibility under injection conditions.

The calculated CO_2 densities range from 555 to 610 kg/m^3 (Table 1). The North Structure, located at greater burial depth (5970 ft–1819.656 m, MD), exhibits the highest CO_2 density (610 kg/m^3), resulting from reservoir conditions of approximately 2585 psi (17.82 MPa) and 70 °C. In contrast, the two reservoir intervals identified within the Central Structure present CO_2 densities of 555 kg/m^3 and 580 kg/m^3, corresponding to reservoir pressures of 1838.1 psi and 1909.5 psi (12.67 and 13.165 MPa), and temperatures of 58.5 °C and 60.8 °C, respectively. Brine densities remain relatively constant, ranging from 1010 to 1013 kg/m^3, maintaining a favorable density contrast for gravitational trapping while reducing buoyancy compared with gaseous CO_2.

Table 1. Thermodynamic conditions and maximum sustainable CO_2 column for the evaluated storage prospects.

Parameter	North Structure	Central, Unit 1	Central, Unit 2
Reservoir depth (MD)	5970 ft–1819.656 m	4245 ft–1293.876 m	4600 ft–1402.08 m
Reservoir pressure	2585 psi–17.82 MPa	1838.1 psi–12.67 MPa	1909.5 psi–13.165 MPa
Reservoir temperature (°C)	70	58.5	60.8
CO_2 density (kg/m^3)	610	555	580
Brine density (kg/m^3)	1010	1013	1010
Maximum CO_2 column	169.1 ft–51.54 m	283.69 ft–86.47 m	270.4–82.42 m

The maximum sustainable CO_2 column was estimated from the capillary entry pressure of the sealing intervals and compared with the structural closure defined from the three-dimensional structural model. The calculated maximum CO_2 columns reach 169.1 ft (51.54 m) for the North Structure and 283.7 ft and 270.4 ft (86.47 and 82.42 m) for the two storage intervals of the Central Structure, indicating that all evaluated seals possess sufficient capillary sealing capacity to retain substantial CO_2 columns.

Although the North Structure exhibits the highest in situ CO_2 density, the Central Structure supports larger capillary-controlled CO_2 columns due to the sealing properties of the overlying mudstone intervals. These results demonstrate that reservoir preference cannot be based exclusively on thermodynamic conditions, since storage security is jointly controlled by CO_2 density, seal capillary entry pressure, and structural closure geometry. Consequently, integrating thermodynamic analysis with capillary seal assessment provides a more comprehensive evaluation of geological storage performance than considering either criterion independently.

4.7. Fault Behavior

Fault behavior represents a critical factor in evaluating the integrity of geological CO_2 storage systems, as faults may either act as effective hydraulic barriers or constitute potential migration pathways depending on their mechanical stability and sealing capacity. In this study, fault behavior was assessed through the integration of geomechanical analysis and fault seal characterization within the geocellular framework, combining fault slip potential (FSP) derived from the Mohr-Coulomb criterion with Shale Gouge Ratio (SGR) modeling. This integrated approach enables the evaluation of fault reactivation susceptibility, sealing efficiency, and the overall risk of fault-controlled CO_2 migration under projected injection conditions.

4.7.1. Fault Slip Potential (FSP)

Fault Slip Potential (FSP), estimated using the Mohr-Coulomb failure criterion within the geomechanical model, was used to identify intervals susceptible to fault reactivation within the Mugrosa Formation. The calculated FSP values range between 0 and 2. Intervals

with FSP values between 0 and 1 indicate higher fault reactivation susceptibility, whereas values greater than 1 suggest mechanically stable conditions with low reactivation potential.

In the North Structure, the interval calibrated with the Zarzal-2 well within the shallowest section of the Mugrosa Formation (5700–6200 ft) exhibits low susceptibility to fault reactivation. Similarly, in the area calibrated with the Coyote-1 well, corresponding to the 3600–4000 ft interval, no significant evidence of fault reactivation susceptibility was identified.

For the Central Structure, the calibration performed for both the reservoir intervals and their associated sealing units within the Mugrosa Formation indicates stable mechanical conditions, with no intervals showing critical fault slip potential (Figure 17). These results suggest that the evaluated faults are unlikely to experience reactivation under the modeled stress and pore-pressure conditions associated with the proposed CO_2 injection scenarios.

Overall, the FSP analysis indicates favorable geomechanical conditions for CO_2 storage, as the main structural discontinuities remain below critical reactivation thresholds. This behavior supports the integrity of the reservoir-seal system and reduces the likelihood of injection-induced leakage through fault-controlled pathways.

4.7.2. Fault Seal Analysis: Shale Gouge Ratio (SGR)

Shale Gouge Ratio (SGR) is a commonly used parameter for evaluating the sealing capacity of faults by estimating the proportion of clay-rich material incorporated into the fault zone during displacement. This parameter is particularly relevant for assessing whether a fault may behave as an effective hydraulic barrier to fluid flow, including the migration of injected CO_2.

Figure 18 presents the spatial distribution of SGR values using a color scale ranging from violet for low values (<0.35) to red for high values (>0.75). High SGR values, predominantly represented by yellow to red tones, indicate an increased shale content within the fault gouge, which is potentially associated with lower fault permeability and enhanced sealing capacity.

The North Structure prospect, associated with the Infantas Fault, exhibits inverse kinematics, with westward vergence and a dip of 40° to 70°. The modeled SGR distribution shows consistently high values along the fault plane, suggesting favorable sealing conditions. In particular, the fault intervals corresponding to the Mugrosa Formation exhibit SGR values between 0.8 and 0.9, indicating a high proportion of clay-rich gouge material. These results imply a reduced probability of vertical CO_2 migration through the fault zone and support the interpretation of the Infantas Fault as an effective sealing structure under the evaluated storage conditions.

The high SGR values identified within the reservoir-seal interval reinforce the integrity of the structural trap and suggest that fault-related leakage risk is relatively low in the evaluated sector. Consequently, the fault seal analysis supports the suitability of the North Structure as a potential candidate for geological CO_2 storage.

Similarly, the Central Structure prospect, associated with the Arrugas Fault, which has a SW-NE bearing with a dip of 34°, also exhibits high SGR values exceeding 0.75, indicating strong fault-sealing potential. The intervals corresponding to the evaluated reservoir and sealing units within the Mugrosa Formation present average SGR values close to 0.85, suggesting a significant proportion of clay-rich gouge material associated with low fault permeability and enhanced sealing capacity (Figure 19).

The heterogeneous distribution of SGR values along the fault plane suggests spatial variability in sealing behavior. Such variability is likely related to lithological contrasts within the displaced stratigraphic intervals, fault geometry, and the tectonic processes that controlled fault evolution and gouge development. These heterogeneities may locally influence fluid migration pathways and pressure compartmentalization within the reservoir-seal system.

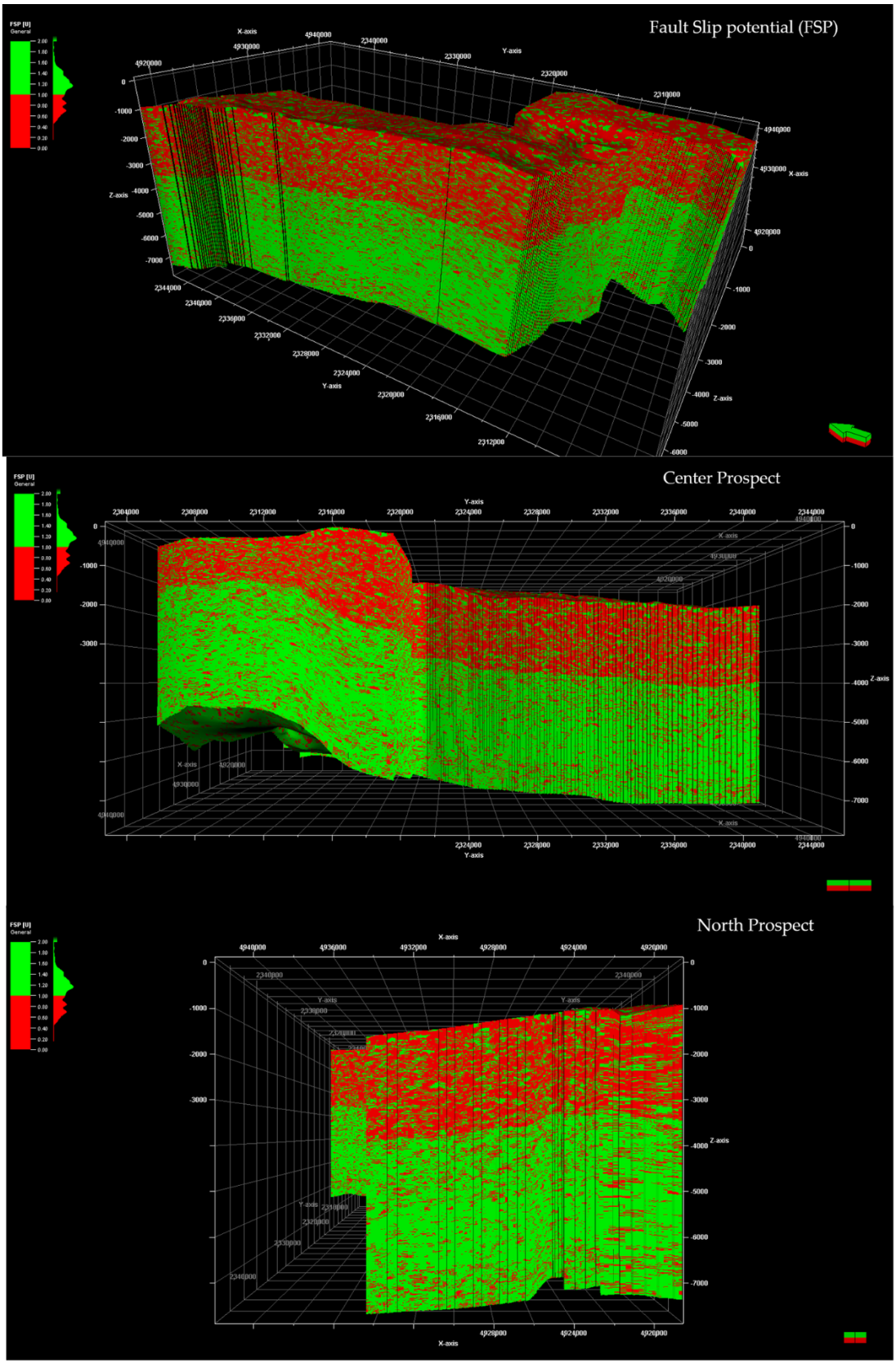


Figure 17. Fault Slip Potential (FSP) distribution populated within the 3D geological model. The model illustrates the spatial variability of fault reactivation susceptibility across the reservoir-seal system based on the Mohr-Coulomb failure criterion. Intervals with FSP values greater than 1 indicate mechanically stable conditions with low fault reactivation potential under the evaluated CO_2 injection scenarios.

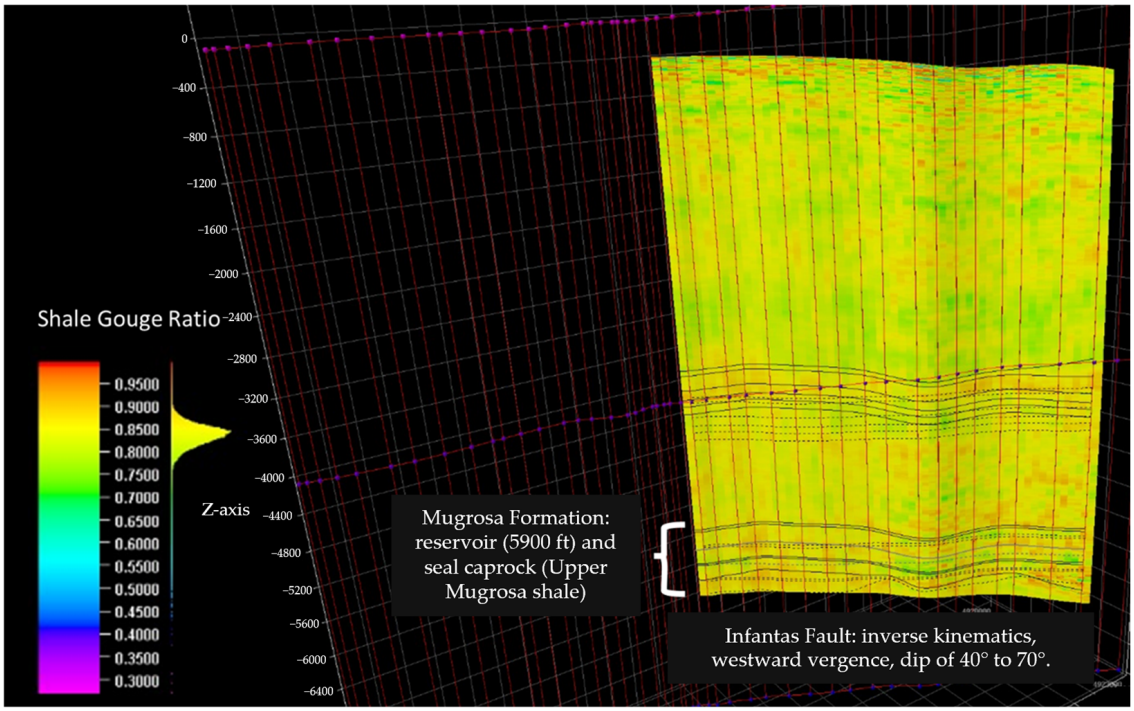


Figure 18. Three-dimensional distribution of Shale Gouge Ratio (SGR) values along the modeled fault planes within the North Structure prospect study area. Warmer colors indicate higher SGR values and therefore greater clay content within the fault gouge, suggesting enhanced sealing capacity and lower fault permeability. The Mugrosa Formation intervals associated with the Infantas Fault exhibit consistently high SGR values, supporting favorable CO_2 containment conditions.

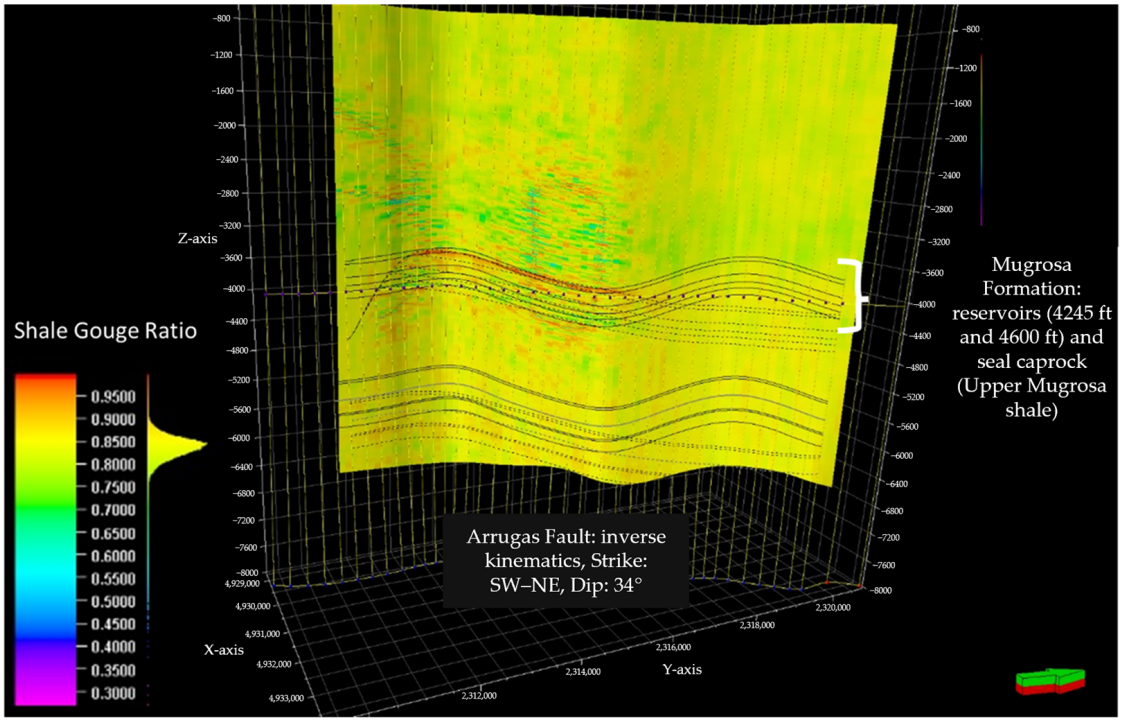


Figure 19. Spatial distribution of Shale Gouge Ratio (SGR) values along the Arrugas Fault within the Central Structure prospect. High SGR values (>0.75) dominate the evaluated fault intervals, suggesting the development of clay-rich fault gouge that may favor low-permeability conditions and enhanced sealing capacity. Local variations in SGR distribution reflect lithological heterogeneity and structural complexity along the fault plane.

Despite this variability, the predominance of high SGR values across the evaluated fault segments indicates that the Arrugas Fault likely behaves as an effective hydraulic barrier under the modeled conditions. Consequently, the structural configuration of the Central Structure appears favorable for long-term CO_2 containment, with a relatively low probability of fault-controlled leakage.

4.7.3. Implications for Storage Integrity

The integrated structural, petrophysical, geomechanical, and capillary seal analyses indicate that both evaluated prospects satisfy the principal geological requirements for long-term CO_2 storage, although each structure exhibits different advantages that influence storage performance and containment security.

The North Structure benefits from deeper burial conditions, resulting in the highest reservoir pressure and temperature among the evaluated prospects. These conditions produce the highest calculated in situ CO_2 density (610 kg/m^3), improving volumetric storage efficiency while reducing buoyancy-driven migration. Furthermore, the Infantas Fault exhibits high SGR values and low fault reactivation susceptibility, indicating favorable fault-sealing behavior. The estimated maximum sustainable CO_2 column of approximately 169 ft confirms that the capillary sealing capacity of the overlying seal is sufficient to maintain CO_2 confinement under the evaluated reservoir conditions.

The Central Structure, despite exhibiting slightly lower CO_2 densities (555–580 kg/m^3), presents the largest calculated capillary-supported CO_2 columns (approximately 270–284 ft). These results suggest that the sealing intervals associated with the Arrugas Fault possess excellent capillary sealing capacity. However, the greater lithological heterogeneity and structural compartmentalization identified within this prospect may introduce local variations in injectivity, pressure propagation, and reservoir connectivity, potentially increasing operational complexity during large-scale CO_2 injection.

The predominance of clay-rich facies throughout the Mugrosa Formation constitutes an important advantage for storage security by providing effective sealing intervals characterized by low permeability and high capillary entry pressures. Nevertheless, the same lithological characteristics reduce reservoir quality by limiting the lateral continuity of high-permeability sandstone bodies, thereby restricting effective storage capacity and potentially affecting injection efficiency.

Overall, the results indicate that the principal uncertainty associated with geological CO_2 storage in the Mugrosa Formation is not related to seal failure through the caprock matrix, but rather to the heterogeneous distribution of reservoir-quality sandstones and the resulting variability in pressure communication within the reservoir. Consequently, reliable prospect evaluation requires integrating thermodynamic conditions, reservoir architecture, capillary seal capacity, fault-sealing behavior, and geomechanical stability into a unified assessment framework.

The integrated workflow developed in this study demonstrates that combining these complementary datasets substantially reduces uncertainty during the screening of geological CO_2 storage sites and provides a more robust basis for prospect ranking than approaches based solely on structural or petrophysical criteria.

5. Discussion

The integrated evaluation performed in this study demonstrates that the feasibility of geological CO_2 storage within the Mugrosa Formation is strongly controlled by the interaction between structural configuration, reservoir heterogeneity, fault-sealing behavior, and geomechanical stability. Although the evaluated prospects exhibit favorable sealing

conditions and structurally closed traps, variations in reservoir quality and fault-related compartmentalization introduce important operational and containment uncertainties.

5.1. Feasibility of Geological CO_2 Storage in the Mugrosa Formation

The results obtained in this study indicate that the Mugrosa Formation presents mixed but generally favorable conditions for geological CO_2 storage. From a structural perspective, both the North and Central prospects correspond to fault-bounded anticlinal traps associated with reverse fault systems, representing a classical structural confinement mechanism commonly considered suitable for subsurface fluid storage.

The North Structure is characterized by comparatively lower structural compartmentalization and greater lateral continuity of reservoir intervals, conditions that may favor pressure dissipation and improve injectivity performance during CO_2 injection. In contrast, the Central Structure exhibits greater heterogeneity in the spatial distribution of porosity and permeability, which may reduce storage efficiency and increase operational complexity due to localized variations in flow behavior and reservoir connectivity.

However, the high clay content identified throughout significant portions of the Mugrosa Formation represents a critical trade-off for storage performance. While clay-rich intervals improve sealing efficiency and contribute to containment integrity, they also reduce effective porosity and permeability, limiting the effective storage capacity and potentially restricting injectivity. Consequently, the feasibility of CO_2 storage within the Mugrosa Formation is strongly controlled by the spatial distribution and connectivity of sandstone-dominated intervals within the reservoir architecture.

Overall, the integrated results suggest that the Mugrosa Formation constitutes a potentially viable target for geological CO_2 storage, although successful implementation would require careful management of injection pressures, detailed characterization of reservoir heterogeneity, and continuous assessment of fault stability to minimize uncertainty associated with long-term containment performance.

5.2. Geomechanical Risks and Fault Stability

The geomechanical analysis indicates that the principal faults associated with the evaluated prospects, namely the Infantas Fault in the North Structure and the Arrugas Fault in the Central Structure, exhibit mechanical conditions that reduce the likelihood of fault reactivation under moderate CO_2 injection pressures. The calculated fault slip potential (FSP) values remain below critical thresholds across the evaluated reservoir intervals, suggesting that the current stress regime is compatible with stable injection conditions.

Nevertheless, the Central Structure exhibits greater structural compartmentalization and increased seismic reflector tortuosity, which may indicate reduced continuity of the sealing intervals. Although the Shale Gouge Ratio (SGR) results suggest that both faults possess favorable sealing characteristics, local discontinuities within the sealing units could potentially facilitate slow fluid migration if injection pressures are not carefully controlled and monitored over time.

The upper and lower sealing intervals identified within the Mugrosa Formation display relatively high Young's modulus values and low permeability, supporting their role as mechanically competent and hydraulically effective barriers. However, the lithological heterogeneity observed in the Central Structure may increase the risk of localized leakage pathways, particularly in areas where the lower sealing units are in direct contact with reservoir sand bodies. These local heterogeneities highlight the importance of detailed site characterization and continuous integrity assessment during storage operations.

Despite these differences, both prospects exhibit sealing conditions supported by the presence of clay-rich intraformational intervals and fault zones with high SGR values,

suggesting a relatively low probability of fault-controlled leakage under the evaluated conditions. Furthermore, the geomechanical analysis indicates that the main structural discontinuities remain below critical reactivation thresholds, reinforcing the potential viability of the reservoir-seal system for CO_2 containment.

In this context, the Central Structure may require a more comprehensive monitoring strategy due to its greater structural complexity and variability in petrophysical properties. Advanced monitoring techniques, including time-lapse (4D) seismic surveys and zonal injection testing, could provide valuable information regarding pressure evolution, plume migration, and reservoir response during injection. The implementation of these monitoring approaches would improve the ability to detect early changes in reservoir behavior and reduce uncertainty associated with long-term CO_2 containment performance.

5.3. Implications of Seal Analysis (SGR) in Heterogeneous Systems

The Shale Gouge Ratio (SGR) is widely used as a first-order predictor of fault-sealing capacity in hydrocarbon-bearing sedimentary basins [8,30]. The SGR calculations assume predominantly reverse (dip-slip) fault kinematics, whereby the measured vertical throw adequately represents the stratigraphic thickness involved in fault gouge generation. Seismic interpretation of both the Infantas and Arrugas faults indicates reverse fault geometries associated with compressional tectonic framework of the Middle Magdalena Valley Basin. Although previous tectonic studies have suggested that minor oblique- or strike-slip deformation may locally occur within the basin [31], no seismic evidence of a significant strike-slip component was identified within the faults analyzed in this study. Nevertheless, potential oblique-slip displacement represents an additional source of uncertainty in SGR-based fault seal predictions and should be considered where detailed structural analyses indicate more complex fault kinematics.

In the present study, SGR analysis suggests that the major faults within the study area generally exhibit favorable conditions for CO_2 containment due to the high clay content present within the displaced stratigraphic units. The predominance of elevated SGR values along both the Infantas and Arrugas faults indicates the development of clay-rich fault gouge zones associated with reduced permeability and enhanced sealing behavior.

However, the results also reveal an important limitation of fault seal prediction in heterogeneous depositional systems. The spatial variability of lithofacies within the Mugrosa Formation produces significant heterogeneity in SGR distribution along the fault planes, implying that sealing capacity is not uniform throughout the fault system. In particular, intervals dominated by shale-rich lithologies tend to generate higher SGR values and therefore more effective sealing conditions, whereas sandstone intercalations may locally produce segments with comparatively lower sealing capacity.

These results highlight the importance of evaluating fault seal behavior at a local scale rather than relying exclusively on regional-scale interpretations, especially in heterogeneous fluvial systems such as the Mugrosa Formation. Local variations in lithological juxtapositions, reservoir connectivity, and fault gouge composition may significantly influence fluid migration pathways and pressure compartmentalization during CO_2 injection.

Although originally developed and calibrated for hydrocarbon systems, SGR should not be interpreted as an absolute criterion for CO_2 containment. Geological CO_2 storage systems are governed by different interfacial tension, wettability, and capillary pressure relationships than conventional hydrocarbon-water systems [3,32].

For this reason, the fault seal analysis was complemented with capillary breakthrough pressure calculations based on seal capillary properties, providing an independent line of evidence to assess seal performance through the estimation of the maximum sustainable CO_2 column. This complementary approach reduces uncertainty in the evaluation of CO_2

containment by incorporating the capillary behavior of the CO_2-brine system, which is not explicitly captured by SGR alone.

Consequently, although the overall SGR results support favorable containment conditions, fault seal integrity for geological CO_2 storage should be evaluated using multiple complementary approaches. Integrating SGR with capillary breakthrough pressure analysis, reservoir characterization, and geomechanical assessment provides a more robust framework for evaluating long-term containment performance, particularly in heterogeneous fluvial systems where lithological variability strongly controls fault- sealing behavior and pressure compartmentalization.

5.4. Implications for Prospect Selection in CCS Projects

The results of this study demonstrate that site selection for geological CO_2 storage in mature sedimentary basins requires a careful balance between storage site capacity and containment security. In the evaluated case, the Mugrosa Formation exhibits favorable sealing conditions associated with clay-rich intraformational seals and fault zones characterized by high SGR values, suggesting a generally reliable containment system. However, these favorable sealing conditions are accompanied by limitations in reservoir quality, including reduced effective porosity, heterogeneous permeability distribution, and compartmentalization associated with structural complexity.

The evaluated prospects also highlight the importance of considering fault behavior under injection conditions as a key component of storage feasibility assessment. Although the geomechanical analysis indicates relatively low fault reactivation susceptibility under moderate injection pressures, the presence of heterogeneous lithologies and structurally compartmentalized intervals may locally influence pressure propagation and fluid migration pathways.

Consequently, the viability of CO_2 storage within the Mugrosa Formation strongly depends on the accurate identification and characterization of connected sandstone bodies capable of sustaining injectivity and storage efficiency. Similarly, maintaining controlled injection pressures is essential to minimize the risk of fault reactivation and preserve seal integrity during long-term operations.

A comparable behavior has been reported in several internationally recognized CCS projects hosted in structurally complex siliciclastic reservoirs, where storage feasibility depends on achieving an appropriate balance between injectivity, seal integrity, and geomechanical stability [3,32].

For example, projects such as the Sleipner field in the North Sea [33], the In Salah project in Algeria [34], and the Quest project in Canada [35] demonstrate that successful long-term CO_2 storage can be achieved even in heterogeneous systems, provided that injection pressures are carefully controlled and reservoir architecture is thoroughly characterized.

Compared with these large-scale projects, the Mugrosa Formation presents comparatively lower reservoir quality due to its higher clay content and stronger compartmentalization, which may limit effective storage capacity and injectivity. However, the evaluated system also exhibits important advantages, including the presence of thick sealing intervals, structurally closed traps, and faults with high SGR values indicative of favorable sealing behavior.

Operationally, the main challenges for the Mugrosa Formation are likely associated with pressure management, uncertainty related to fault-controlled migration, and the identification of laterally connected sandstone bodies capable of sustaining stable injection rates. These characteristics position the Mugrosa Formation as a technically promising,

though operationally complex, candidate for future CCS development within mature Andean basins.

The workflow presented here is intended to support the early stages of CCS site screening and prospect ranking. Quantitative storage capacity estimation requires additional characterization, including gross rock volume, net-to-gross ratio, storage efficiency factors, and dynamic reservoir simulations, which were beyond the scope of the present study. Nevertheless, the integrated geological and geomechanical characterization developed herein provides the essential framework for subsequent capacity estimation and injection design.

These results emphasize that prospect selection in CCS projects should not rely exclusively on reservoir capacity estimates, but rather on an integrated evaluation of structural configuration, fault-sealing behavior, reservoir heterogeneity, and geomechanical stability. In structurally complex and heterogeneous systems such as the Middle Magdalena Valley Basin, multidisciplinary workflows integrating seismic interpretation, geocellular modeling, geomechanics, and fault seal analysis are essential to reduce uncertainty and improve decision-making during early-stage CCS project screening.

6. Conclusions

This study developed an integrated geocellular modeling workflow for evaluating the appropriateness of the Mugrosa Formation within the Middle Magdalena Valley Basin for geological CO_2 storage. The proposed methodology integrates structural interpretation, sedimentological and petrophysical characterization, fault seal analysis, and geomechanical assessment within a unified modeling framework, allowing a comprehensive evaluation of reservoir-seal integrity under prospective CO_2 injection conditions.

The multicriteria ranking workflow enabled the identification of two priority prospects, namely the North Structure and the Central Structure. Among them, the North Structure exhibits comparatively more favorable conditions due to its greater reservoir continuity, lower structural compartmentalization, and more effective structural confinement associated with the Infantas Fault system. In contrast, the Central Structure presents greater operational and geological challenges related to lithological heterogeneity and spatial variability in petrophysical properties, which may affect injectivity and the homogeneous distribution of injected CO_2. Additionally, the direct interaction between reservoir intervals and structural discontinuities locally increases uncertainty regarding potential migration pathways and long-term containment performance.

Petrophysical characterization indicates that the Mugrosa Formation is dominated by clay-rich facies, resulting in generally limited reservoir quality. Consequently, the effective storage potential is restricted to discrete sandstone bodies characterized by heterogeneous spatial distribution and variable connectivity. These results demonstrate that reservoir continuity and connectivity constitute primary controls on storage feasibility within the evaluated system.

Fault seal analysis suggests generally favorable containment conditions due to the high clay content present within the displaced stratigraphic units, promoting the development of sealing fault gouge materials with elevated SGR values. However, the heterogeneous nature of the depositional system introduces significant local variability in sealing capacity, indicating that fault behavior must be evaluated at both regional and local scales.

The geomechanical analysis indicates that the principal faults, namely the Infantas Fault in the North Structure and the Arrugas Fault in the Central Structure, remain mechanically stable under moderate injection pressures, supporting the preservation of fault-sealing capacity during injection scenarios. Nevertheless, the lithological heterogeneity identified within the sealing intervals of the Central Structure may represent an additional long-term integrity risk, particularly in intervals characterized by lower cohesion or localized mechan-

ical weakness, where slow fluid migration could potentially occur if injection pressures are not adequately managed.

Overall, the results demonstrate that the viability of geological CO_2 storage within the Mugrosa Formation is controlled not only by seal integrity, but fundamentally by the quality, continuity, and connectivity of the reservoir intervals. This highlights the importance of integrating sedimentological, petrophysical, structural, and geomechanical analyses during the early stages of CCS prospect evaluation.

Finally, the proposed workflow provides a reproducible and adaptable methodology for the geological screening and suitability assessment of potential CO_2 storage sites assessment in sedimentary basins characterized by significant heterogeneity and limited data availability. The methodology may therefore provide a valuable framework for future CCS screening and feasibility studies in mature Colombian basins and analogous geological settings worldwide. The resulting structural, petrophysical, and geomechanical models constitute the basis for subsequent storage capacity estimation and dynamic injection simulations.

Author Contributions: Conceptualization, E.H.O.; Methodology, E.H.O.; Software, E.H.O.; Validation, E.H.O. and M.C.R.C.; Formal analysis, E.H.O. and M.C.R.C.; Investigation, E.H.O.; Resources, M.C.R.C.; Data curation, E.H.O.; Writing—original draft, E.H.O.; Writing—review and editing, E.H.O. and M.C.R.C.; Visualization, E.H.O. and M.C.R.C.; Supervision, E.H.O. and M.C.R.C.; Project administration, E.H.O. and M.C.R.C. All authors have read and agreed to the published version of the manuscript.

Funding: This research received no external funding.

Data Availability Statement: The original contributions presented in this study are included in the article. Further inquiries can be directed to the corresponding author.

Acknowledgments: During the preparation of this manuscript, the author(s) used ChatGPT (GPT-5.6) for the purposes of English language editing, translation, grammar correction, refinement of scientific wording, restructuring of selected passages, and improvement of the clarity and readability of the manuscript. The authors have reviewed and edited the output and take full responsibility for the content of this publication.

Conflicts of Interest: The authors declare no conflict of interest.

Abbreviations

The following abbreviations are used in this manuscript:

MMVB	Middle Magdalena Valley Basin
SGR	Shale Gouge Ratio
CCS	Carbon Capture and Storage
CCUS	Carbon Capture, Utilization and Storage
GR	Gamma Ray
SP	Spontaneous Potential
RHOB	Bulk Density
NPHI	Neutron Porosity
LOT	Leak-Off Test
Vsh	Shale Volume
PHIT	Total Porosity
CALI	Caliper

References

1. IPCC. *Informe Especial Sobre Captura y Almacenamiento de Dióxido de Carbono*; Cambridge University Press: Cambridge, UK, 2005.
2. Holloway, S. An overview of the underground disposal of carbon dioxide. *Energy Convers. Manag.* **1997**, *38*, S193–S198. [CrossRef]

3. Benson, S.M.; Cole, D.R. CO_2 sequestration in deep sedimentary formations. *Elements* **2008**, *4*, 325–331. [CrossRef]
4. Bachu, S.S. CO_2 storage in geological media: Role, means, status and barriers to deployment. *Prog. Energy Combust. Sci.* **2008**, *34*, 254–273. [CrossRef]
5. Song, Y.; Jun, S.; Na, Y.; Kim, K.; Jang, Y.; Wang, J. Geomechanical challenges during geological CO_2 storage: A review. *Chem. Eng. J.* **2023**, *456*, 140968. [CrossRef]
6. Birkholzer, J.; Zhou, Q.; Tsang, C.F. Large-scale impact of CO_2 storage in deep saline aquifers: A sensitivity study on pressure response in stratified systems. *Int. J. Greenh. Gas. Control* **2009**, *3*, 181–194. [CrossRef]
7. Dommisse, R.R. Constraining faults and stratigraphic zones in shale and tight oil basins via 3D geocellular models. *Geoenergy Sci. Eng.* **2024**, *240*, 212991. [CrossRef]
8. Yielding, G.; Freeman, B.; Needham, D.T. Quantitative fault seal prediction. *AAPG Bull.* **1997**, *81*, 897–917. [CrossRef]
9. Pan, P.; Wu, Z.; Feng, X.; Yan, F. Geomechanical modeling of CO_2 geological storage: A review. *J. Rock. Mech. Geotech. Eng.* **2016**, *8*, 936–947. [CrossRef]
10. Xue, Y.; Wang, L.; Cao, Z.; Xie, H.; Ranjith, P.G.; Cai, C. Thermo-mechanical degradation and crack evolution of granite subjected to liquid nitrogen cooling cycles for thermal reservoir stimulation. *J. Rock. Mech. Geotech. Eng.* **2026**, *18*, 3447–3470. [CrossRef]
11. Cao, Z. The Bifurcation Characteristics and Dynamical Evolution Rule of Non-Isothermal Seepage Mechanical Model in Fractured Rock Mass. *Processes* **2026**, *14*, 1985. [CrossRef]
12. Yáñez Angarita, E.; Núñez-López, V.; Ramírez Ramírez, A.; Castillo Monroy, E.; Faaij, A. Rapid screening and probabilistic estimation of the potential for CO_2-EOR and associated geological CO_2 storage in Colombian petroleum basins. *Pet. Geosci.* **2022**, *28*, 32606–32621. [CrossRef]
13. Lozano, E.; Zamora, N. *Anexo N—Compilación de La Cuenca del Valle Medio del Magdalena*; Servicio Geológico Colombiano: Bogotá, Colombia, 2014. Available online: https://recordcenter.sgc.gov.co/B20/23008100024725/Documento/Pdf/2105247251114000.pdf (accessed on 10 September 2025).
14. Sarmiento-Pérez, G.; Puentes, J.; Sierra, C. Evolución Geológica y Estratigrafía del Sector Norte del Valle Medio del Magdalena. *Geol. Norandina* **2015**, *12*, 51–82.
15. Montgomery, S. Petroleum potential of Upper and Middle Magdalena basins, Colombia. *Pet. Front.* **1992**, *9*, 67.
16. Moreno, C.J.; Horton, B.K.; Caballero, V.; Mora, A.; Parra, M.; Sierra, J. Depositional and provenance record of the Paleogene transition from foreland to hinterland basin evolution during Andean orogenesis, northern Middle Magdalena Valley Basin, Colombia. *J. S. Am. Earth Sci.* **2011**, *32*, 246–263. [CrossRef]
17. Sarmiento, L.F. *Petroleum Geology of Colombia. Middle Magdalena Basin*; Agencia Nacional de Hidrocarburos (ANH): Bogotá, Colombia, 2011; Volume 11.
18. Caballero Ortiz, V.M. *Evolución Tectono-Sedimentaria del Sinclinal de Nuevo Mundo, Cuenca Sedimentaria Valle Medio del Magdalena Colombia, Durante el Oligoceno-Mioceno*; Universidad Industrial de Santander: Santander, Colombia, 2010.
19. Royero, J.M.; Clavijo, J. *Mapa Geológico Generalizado del Departamento de Santander*; INGEOMINAS: Bogotá, Colombia, 2001.
20. Mojica, J.; Franco, R. Estructura y evolución tectónica del Valle Medio del Magdalena, Colombia. *Geol. Colomb.* **1990**, *17*, 41–64.
21. Cooper, M.A.; Addison, F.T.; Alvarez, R.; Coral, M.; Graham, R.H.; Hayward, A.B.; Howe, S.; Martinez, J.; Naar, J.; Peñas, R.; et al. Basin development and tectonic history of the Llanos Basin, Eastern Cordillera, and Middle Magdalena Valley, Colombia. *AAPG Bull.* **1995**, *79*, 1421–1443. [CrossRef]
22. Bachu, S. Sequestration of CO_2 in geological media: Criteria and approach for site selection in response to climate change. *Energy Convers. Manag.* **2000**, *41*, 953–970. [CrossRef]
23. Bachu, S. Screening and ranking of sedimentary basins for sequestration of CO_2 in geological media in response to climate change. *Environ. Geol.* **2003**, *44*, 277–289. [CrossRef]
24. Bachu, S.; Adams, J.J. Sequestration of CO_2 in geological media in response to climate change: Capacity of deep saline aquifers to sequester CO_2 in solution. *Energy Convers. Manag.* **2003**, *44*, 3151–3175. [CrossRef]
25. Petrel. *Property Modeling*; Schlumberger: Houston, TX, USA, 2010. Available online: https://www.slb.com/products-and-services/delivering-digital-at-scale/software/petrel-subsurface-software/petrel/petrel-geology-and-modeling/petrel-petrophysical-modeling (accessed on 10 September 2025).
26. Tamulonis, K. A methodology for integrating unconventional geologic and engineering data into a geocellular model. *Interpretation* **2020**, *8*, 1–71. [CrossRef]
27. Deutsch, C.V.; Journel, A.G. *GSLIB: Geostatistical Software Library and User's Guide*; Oxford University Press: Oxford, UK, 1998.
28. Serra, O. *Fundamentals of Well-Log Interpretation*; Elsevier: Amsterdam, The Netherlands, 1984.
29. Wyllie, M.R.J.; Gregory, A.R.; Gardner, L.W. Elastic Wave Velocities in Heterogeneous and Porous Media. *Geophysics* **1956**, *21*, 41–70. [CrossRef]
30. Yielding, G. Shale Gouge Ratio—Calibration by geohistory. *Nor. Pet. Soc. Spec. Publ.* **2002**, *11*, 1–15. [CrossRef]
31. Reyes, M.; Kley, J.; Mora, A.; Bello-Palacios, D.; Vargas, A.F.; Carvajal-Torres, J.; Osorno, J. Chapter 15—La Cira Basement-high; Middle Magdalena Valley Basin, Colombia. In *Andean Structural Styles*; Elsevier: Amsterdam, The Netherlands, 2022; pp. 207–219.

32. Michael, K.; Golab, A.; Shulakova, V.; Ennis-King, J.; Allinson, G.; Sharma, S.; Aiken, T. Geological storage of CO_2 in saline aquifers—A review of the experience from existing storage operations. *Int. J. Greenh. Gas. Control* **2010**, *4*, 659–667. [CrossRef]
33. Chadwick, A.; Arts, R.; Eiken, O. *4D Seismic Quantification of a Growing CO_2 Plume at Sleipner, North Sea*; Geological Society, London, Special Publications: London, UK, 2004; Volume 233, pp. 1385–1399. [CrossRef]
34. Mathieson, A.; Midgley, J.; Dodds, K.; Wright, I.; Saoul, N.; Ringrose, P. CO_2 sequestration monitoring and verification technologies applied at Krechba, Algeria. *Lead. Edge* **2010**, *29*, 216–222. [CrossRef]
35. Whittaker, S.; Rostron, B.; Hawkes, C.; Gardner, C.; White, D.; Johnson, J.; Chalaturnyk, R.; Seeburger, D. A decade of CO_2 injection into depleting oil fields: Monitoring and research activities of the IEA GHG Weyburn-Midale CO_2 Monitoring and Storage Project. *Energy Procedia* **2011**, *4*, 6069–6076. [CrossRef]

Disclaimer/Publisher's Note: The statements, opinions and data contained in all publications are solely those of the individual author(s) and contributor(s) and not of MDPI and/or the editor(s). MDPI and/or the editor(s) disclaim responsibility for any injury to people or property resulting from any ideas, methods, instructions or products referred to in the content.